Horizon 2020
European Union Funding
for Research & Innovation

DELIVERABLE D3.4

SOFC stack testing report

DISSEMINATION LEVEL: CONFIDENTIAL

Grant Agreement (GA) N. 85284

Research and Innovation Actions (RIA) project

Granted by:

Innovation and Networks Executive Agency (INEA)

Document Control Sheet

Project	**BLAZE** - Biomass Low cost Advanced Zero Emission small-to-medium scale integrated gasifier-fuel cell combined heat and power plant
Grant Agreement n.	85284
Document Title	D3.4 SOFC stack testing report
Lead Beneficiary	SP_YV , EPFL, ENEA
WP number	D3.4
Type	Report
Dissemination level	C: Confidential

Version	**Date**	**Description**
V0	7/7/2023	First draft for revision
V1	18/7/2023	Revised
V2	7/8/2023	Final version

Date	18/07/2023
Number of pages	65
Archive name	D3.4
Authors	Stefan Diethelm, Audrey Wesoly
Contributors	Florian Berset, Pierre-Yves Aubertin, David Constantin, Jan Van herle
Reviewer(s)	Jan Pieter Ouweltjes (SolydEra)

TABLE OF CONTENT

This project has received funding from the European Union's Horizon 2020 research and innovation programme under grant agreement No 815284

LIST OF FIGURES

LIST OF TABLES

1 EXECUTIVE SUMMARY

In the frame of T3.4, three short stacks from the manufacturer SolydEra were tested under simulated syngas produced by the steam gasification of woody biomass. The goal was to address the impact of impurities contained in the syngas, namely tars (**toluene** and naphthalene), sulfur compounds (**DMS** was injected, which decomposes in H_2S at the stack temperature) and halogens (**HCl**) (as identified in D3.2) on the performance of the short stacks. The impurities were added using a stepwise increase of concentration that ranged from **0.2 ppm to 4 ppm** all tests included.

The stacks are made of 6 repeating units including 6 Ni-YSZ anode-supported cells of 80 cm^2 active area. The potential of each repeating unit were measured and electrochemical impedance spectroscopy (EIS) measurements have been conducted before each new level of contamination. Distribution of relaxation times (DRT) was used to deconvolute individual processes. The fuel inlet and outlet gas compositions of the stacks were also analysed by two different gas chromatographs.

The first stack ran **9000 h**. At the beginning, the evaporator parameters were tuned and a degradation benchmark of -3.4 mV/kh was measured. In the meantime, the methodology for the injection of impurities, including calibration, was developed. Naphthalene turned out to be very challenging to inject due to its solid nature at room temperature, both in the stack and in the gas chromatograph. This stack was finally exposed to 0.5 ppm DMS during 200 h. After 70 h without degradation, the individual cells lost 30 mV in 80 h.

The second stack also ran **9000 h in total**. After obtaining a baseline performance under synthetic woodgas conditions (benchmark degradation rate of -5.73 mV/kh), sulfur was added to the mix. Concentrations went from 0.2 ppm to 1.4 ppm, using steps of 0.2 ppm. The onset of degradation occurred 25 h after the exposure. For all levels of DMS, a first voltage drop was followed by a linear degradation. At the first sulfur level of 0.2 ppm, voltages dropped by 42 mV followed by a linear degradation rate of -21 mV/kh. The last level shows a cumulated voltage drop of 60 mV, followed by a linear degradation rate of -32 mV/kh. Simultaneous exposure to toluene did not produce a significant effect (20 ppm to 180 ppm). The performance loss observed due to the introduction of sulfur has been attributed to the increase in polarization resistance, whereas the ohmic resistance stayed constant. Hansen [10] has shown that S-adsorption follows a Temkin-like isotherm and that the performance loss is linearly proportional to the nickel surface coverage in the anode. Thanks to this method, described in the present document, the surface coverage has been estimated to 70% of the nickel surface before the onset of degradation.

The third stack ran **7000 h** including an initial baseline that shows a benchmark degradation rate of -8.2 mV/kh (-6.9 mV/kh if RU6 is excluded). The sulfur contamination ranged from 0.5 ppm to 4 ppm and it took again 40 h before the onset of degradation at the first level. Similar to stack#2, a first voltage drop was followed by a linear degradation rate. For 0.5 ppm of sulfur, a drop of 37.5mV was recorded, followed by a degradation rate of -13.8 mV/kh. At 4 ppm, the cumulative voltage drop was 69.7 mV and the linear degradation rate -30.4 mV/kh. Impedance spectra were deconvoluted using a Matlab tool reported in [3]. The resulting DRT plot showed 5 peaks, the physics of which were attributed in house by Caliandro [9]. Sulfur poisoning was found to affect DRT peaks under 2 Hz and above 50 Hz. The low frequency peak was attributed to the conversion impedance (P2). This is consistent with the observations from Anke Hagen [9]. Using $H_2/H_2O/CO$ feed mixtures, she had shown that S-poisoning affects the kinetics of the reverse water gas shift reaction (RWGS), thereby modifying the gas composition and resulting in a significant increase of the conversion impedance as measured by EIS. Two higher frequency peaks are also affected; P4 at $3 \cdot 10^2$ to 10^3 Hz that is attributed to charge transfer in the fuel electrode and P5 at $4 \cdot 10^3$ Hz to 10^4 Hz whose attribution doesn't find any consensus in literature. The sulfur surface coverage was estimated similar to stack#2, with the same result. Another observation worth mentioning is that after stopping the injection of impurity, the **stack recovered** 50% of its performance in 33 h and **80% after 250 h**. Total recovery was not reached, even not 2400 h later (76% recovery). A minor positive effect of toluene (100 ppm to 400 ppm) was observed on the conversion peak (P2). It moderates the impact of H_2S as the peak area is decreased at 400 ppm for all H_2S levels. At the end of the test, the anode was exposed to HCl (5 ppm to 50 ppm) during 120 h. The degradation rate was -60 mV/kh for all concentration levels. After the HCl supply was stopped, the performance continued to degrade at -43 mV/kh.

2 INTRODUCTION

2.1 Objectives and scope of the document

The scope of the document is to give a complete overview of the activities carried out by EPFL within T3.4 on the testing of SOFC short stacks under conditions simulating the operation with syngas produced by the steam gasification of woody biomass (woodgas). As for T3.3, which focused on single cell testing at ENEA, this task specifically addresses the impact of impurities contained in the syngas, namely tars, suphur compounds and halogens (as identified in D3.2) on the performance of the short stacks.

The objectives of this document are therefore:

- Investigate the performance of short stacks under synthetic woodgas feed
- Investigate the effect of impurities on the stack performance
- Determine acceptable impurity levels for the gas cleaning requirement

2.2 Structure of the deliverable

Deliverable 3.4 is divided into three parts beside the introduction:

- Chapter 3, in which the test bench used for the testing of the short stacks, the methodology followed to inject the impurities and the tools used for the analysis of the data are described in details;
- Chapter 4, in which the results obtained from the testing of the three short stacks are presented and discussed;
- Conclusions

3 MATERIALS AND METHODS

3.1 Test Bench

The SOFC short stacks used were provided by SOLIDpower which, during the course of the Blaze project changed its name to SolydEra. The short stacks consist of 6 Ni-YSZ anode-supported cells with an active area of 80 cm^2 each. The air electrode is based on (La,Sr)(Fe,Co)$O_{3-\delta}$ perovskite oxide and the metallic interconnecting plates are made of coated ferritic stainless steel. The experimental test setup is schematized in Figure 1.

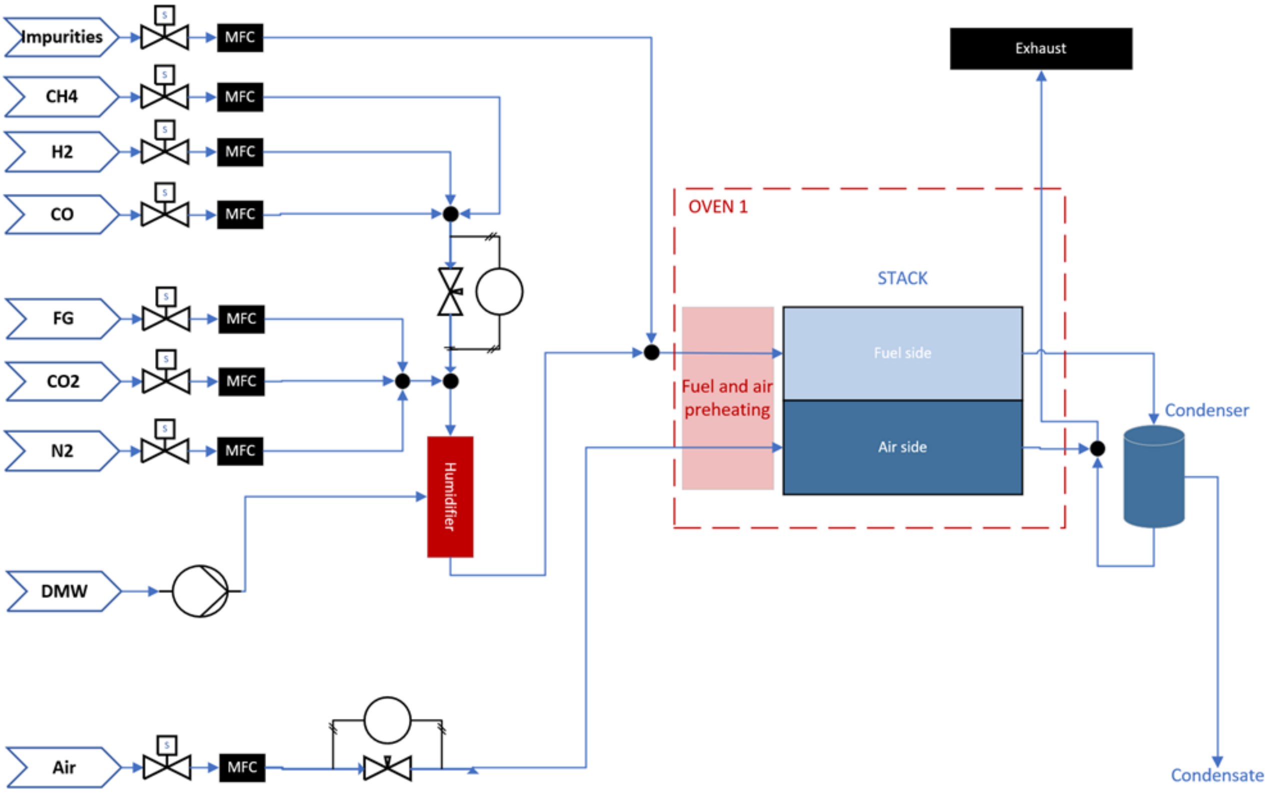

Figure 1: PFD of the testbench used in BLAZE to characterize the short stacks. Refer to text for details.

The short stacks are mounted on a dedicated set-up at EPFL-GEM which delivers and preheats the gases (air, H_2, N_2, CO, CH_4, CO_2, steam) and allows the measurement of gas inlet and outlet temperatures, pressures and the voltage of the individual repeating units (RU). The current is controlled by an electronic load (Elektro-Automatik, Germany), the gas flows with mass-flow controllers (MFC, Voegtlin, Switzerland) and the water feed by a membrane pump (KNF, Germany). Steam is produced in a home-made electrical evaporator. Besides the regular gas feeds that allow to simulate the woodgas composition (H_2, CO, CO_2, CH_4, H_2O), the set-up is equipped with an additional inlet for injecting impurities as shown in Figure 2. An alumina tube is used to prevent the interaction with deliberately added contaminants before reaching the stack. Furthermore, the tubing used at room temperature for the impurities was glass coated to prevent reaction. The simulated woodgas, as given in the next section (BLAZE conditions), was generated using H_2, CO, CO_2, H_2O and CH_4 through mixing to the desired partial pressures by means of the MFCs.

Oil-free compressed air from the lab infrastructure was used. The considered contaminants in the project were H_2S, toluene, naphtalene and KCl. The direct use of H_2S in our laboratory was not possible because of safety issues. Therefore, a less toxic precursor, dimethyl sulfide (DMS), was used from a gas supply bottle of 500 ppm in H_2. This organo-sulfur compound was found to thermally decompose into H_2S in reducing environment above 340 °C, as demonstrated in a separate experiment (cf. Figure 3).

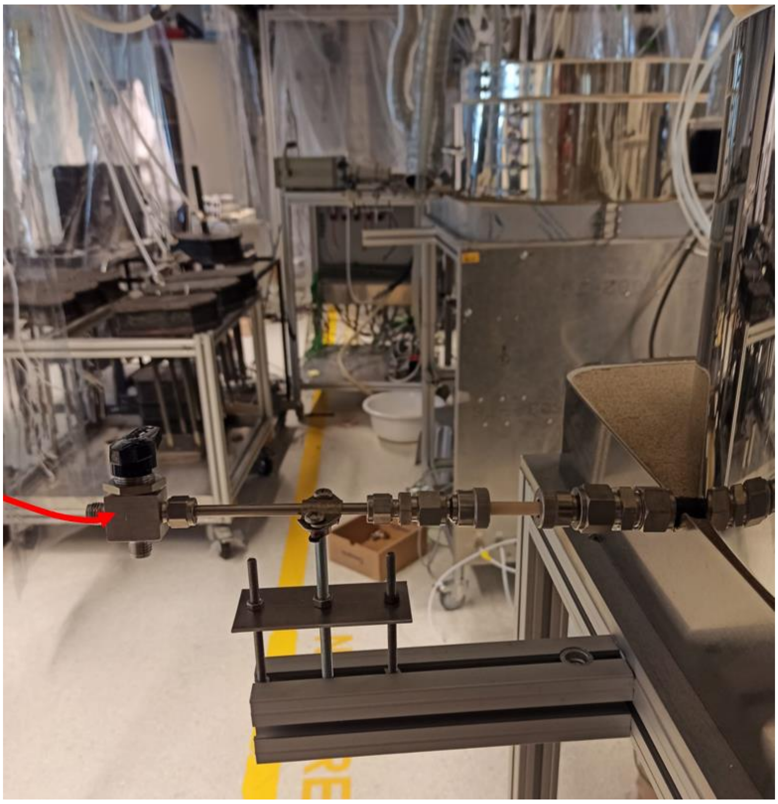

Figure 2: Secondary fuel inlet port for the injection of impurities.

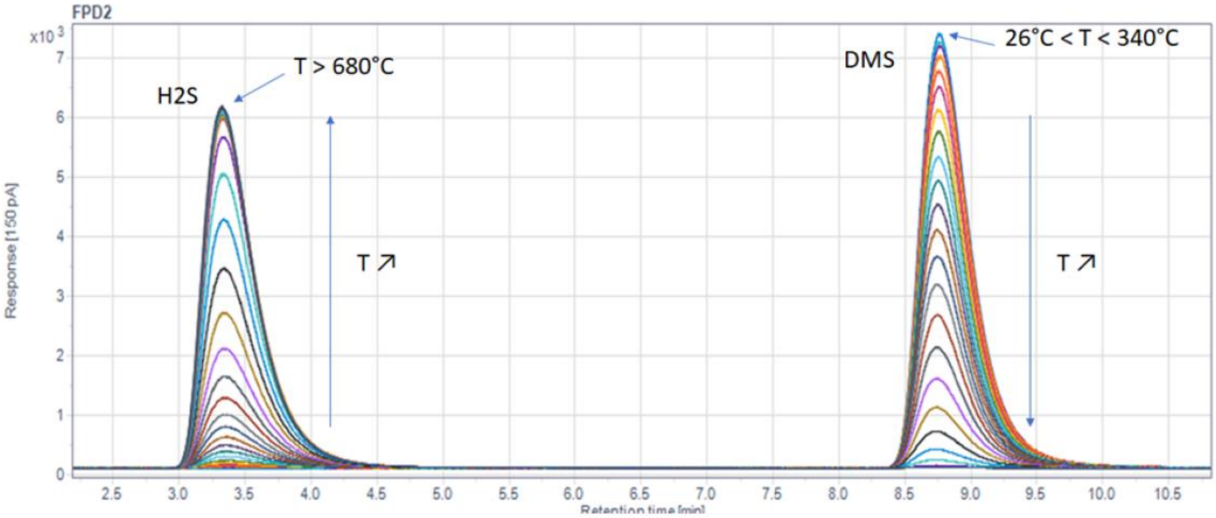

Figure 3: Thermal decomposition of DMS into H_2S in presence of H_2, as a function of temperature, in a quartz reactor filled with quartz wool. Chromatograms measured with an Agilent Gas Chromatograph (GC) equipped with a CP-sil-5 column and a FPD detector (cf. 3.5).

Toluene injection was done by saturating H_2 with toluene contained in a glass bottle maintained in a bath of melting ice at 0 °C. The corresponding vapor pressure is 9 mbar according to Antoine's equation [1].

The adjustment of the impurity level was done by substituting part of the main H_2 feed with the secondary H_2 feed containing impurities.

A similar approach was followed with naphtalene but with a thermal bath set at 60°C since naphtalene is solid at room temperature. However, due to uncontrolled condensation and solidification in the gas chromatograph (GC injector), the introduction of naphtalene to the gas mixture was finally abandoned.

The injection of KCl, intended to measure the impact of both halogens and alkali metals, was finally not pursued either but replaced by HCl diluted in N_2.

The electrochemical impedance spectra (EIS) were recorded using an Zennium X electrochemical workstation (Zahner, Germany) equipped with an active load (EL1000, Zahner).

3.2 Fuel composition

The gas composition (SG1) given in Table 1 was considered to mimic a typical syngas produced by the steam gasification of wood. As CO was only available to a limited extent, it was replaced by H_2, being equivalent in terms of exchanged electrons (SG2). The gas flows were chosen in order to reach 80% fuel utilisation (FU) at 0.4 A/cm^2. The resulting gas compositions and flows are given in Table 1.

Table 1: Synthetic woodgas compositions used within the BLAZE project

	SG1		SG2	
	Composition	**Flows [NL/min]**	**Composition**	**Flows [NL/min]**
H_2	45.0%	1010	69.0%	1548
CO	24.0%	539	0	0
CO_2	11.0%	247	11.0%	247
CH_4	2.0%	45	2.0%	45
H_2O	18.0%	404	18.0%	404

The performance of the short stack was similar with both synthetic woodgas compositions and are overlapping in Figure 4. The initial performance of stack 1 with the reference dry H_2/N_2 composition is also shown for comparison. The presence of steam in the woodgas compositions decreases the oxygen partial pressure difference between the electrodes leading to a smaller open circuit voltage (OCV) but also results in a slight decrease of the area specific resistance (ASR) compared to the dry H_2/N_2 feed.

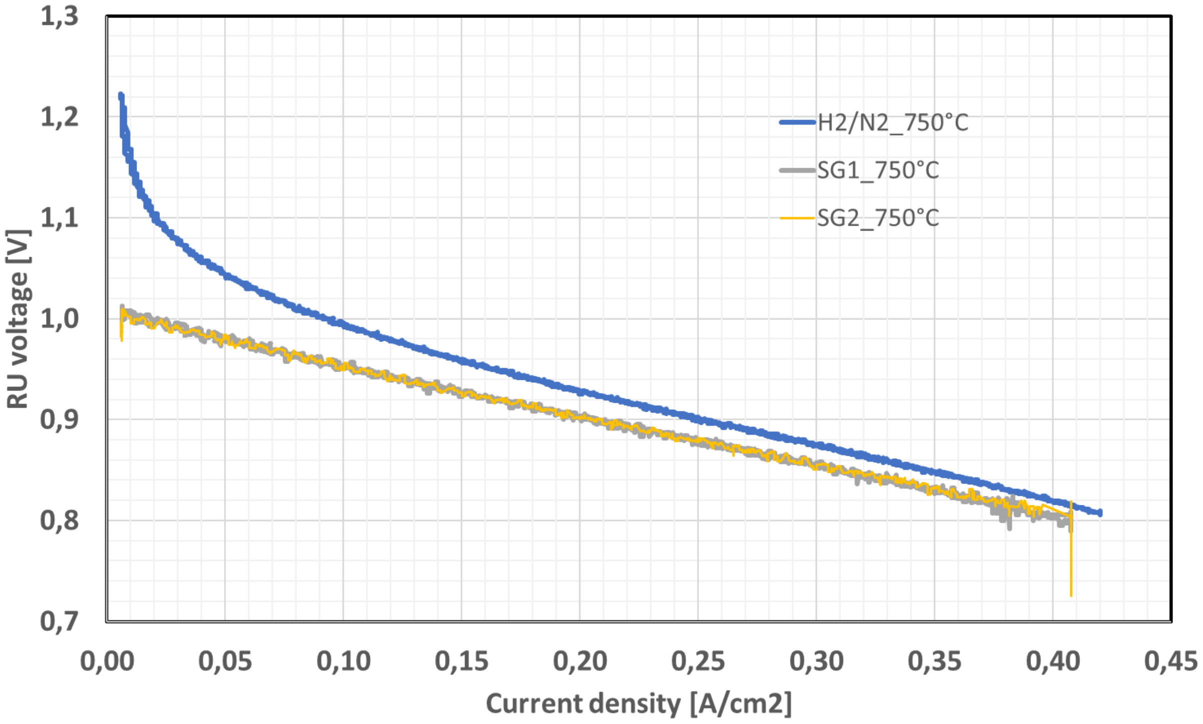

Figure 4: Comparison of the initial V-I performance of stack#1 with the reference H_2/N_2 gas feed and the two synthetic woodgases SG1 and SG2 (cf. Table 1 for composition). All measurements were performed at 750°C and with comparable fuel flows in terms of equivalent number of transferred electrons.

3.3 Method

The short stacks were heated up to 750 °C at a heating rate of 60°C per hour with 2 NL/min of forming gas (5% H_2 in N_2) flowing on the anode side and 32 NL/min of air on the cathode side. Once the stack temperature reached 600 °C, the anode gas was changed to 1.728 NL/min H_2 and 1.152 NL/min N_2 , keeping the same air flow (nominal conditions). An initial V-I characterisation was performed under nominal conditions (750°C air outlet temperature, gases as above) up to 33 A, using a 1 A/min ramp. This V-I was then used to check the health of the stack by comparison with the qualification sheets provided by SOLIDpower/SolydEra. EIS measurements were performed under the same conditions (32A bias) with 1-2 A perturbation, in the frequency range from 100 kHz to 15 mHz. After that, the gas conditions were switched to the BLAZE project conditions (cf. Table 1). The equivalent water flow was 324 µL/min. An V-I was performed under these conditions and EIS measurement taken on each RU. The short stack was then polarized at 32A for >500h for stabilization in order to obtain a reference line. EIS measurements were performed periodically on each RU depending of the test but at least at the beginning and end of the baseline sequence. A steady-bias current of 32 A (0.4 A/cm^2) was maintained throughout the test. It was planned to never set the short stack to OCV (exception made in case of failure and/or emergencies) in order to avoid changing the state of the electrodes. Therefore, to keep the short stack polarised with a constant DC-bias of 32 A, the current applied by the electronic load was gradually decreased to OCV while increasing concurrently that of the EIS device.

3.4 Contaminant exposure

Stack 1:

The stack was contaminated mainly at 0.5 ppm during 200 h.

Stack 2:

The exposure to the contaminants was done in a step-wise increase: for H_2S, a step of 0.2 ppm was used, namely, 0.2, 0.4, 0.6, 0.8,…,1.6 ppm. After long exposure for the initial surface coverage, each level lasted about 100 hours. During each H_2S exposure step, exposure to toluene was added gradually, initially 0, 20, 40 and 60 ppm, then later on, the steps were increased to 60, 120 and 180 ppm since the impact was small. Each toluene exposure step lasted 20 to 24 hours without applying recovery phases in-between.

Stack 3:

The levels of exposure were increased both for H_2S and toluene, namely 0.5, 1, 2, 3 and 4 ppm of H_2S and 0, 100 and 400 ppm of toluene. After 15 weeks of recovery (stack polarised at 32 A under syngas) the stack endured 4 days of contamination with HCl at 5, 10, 20 and 50 ppm.

Table 2: Combination of H_2S and toluene concentrations investigated for stack#2 and stack#3

Stack 2:

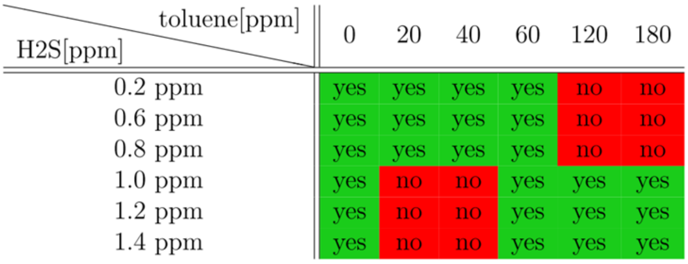

H2S[ppm] \ toluene[ppm]	0	20	40	60	120	180
0.2 ppm	yes	yes	yes	yes	no	no
0.6 ppm	yes	yes	yes	yes	no	no
0.8 ppm	yes	yes	yes	yes	no	no
1.0 ppm	yes	no	no	yes	yes	yes
1.2 ppm	yes	no	no	yes	yes	yes
1.4 ppm	yes	no	no	yes	yes	yes

Stack 3:

H2S [ppm] \ Toluene [ppm]	0	100	400
0,5	yes	yes	yes
1	yes	yes	yes
2	yes	yes	yes
3	yes	yes	yes
4	yes	yes	yes

EIS measurements were performed before and after each exposure step using a constant bias, i.e. without returning to OCV. During the exposure, stack inlet and outlet gas compositions were analyzed at the beginning and end of the exposure sequence.

3.5 Gas analysis

Gas samples were extracted from the inlet and outlet of the stack using syringes (800 µL syringe for sulfur analysis, 50 mL syringe for the permanent gases) and injected for analysis in a gas chromatograph (GC) Agilent ® 8890 equipped with four capillary columns (CP-Sil-5, CP-Sil-8, Poraplot Q and Molecular Sieve 5Å) and three detectors (FPD, FID and TCD). The full range of gases and impurities could thereby be analysed (cf Figure 5). With stack#3, a smaller, mobile GC (Agilent ® 490 Micro-GC) was used for the permanent gases without syringe but directly connected with a T-piece in the gas line.

The calibration data of the FPD detector response to H_2S is shown in Figure 6. In Figure 7, the final calibration points were computed from the mean value of the calibration data. The measurement method shows some limitations. First, the concentration range is a bit high considering the concentration measured during the experiments, which is below 1 ppm, even though the contamination ranges from 0.5 ppm to 4 ppm. Second, it appeared that the quantity of gas collected with the syringe depends on the flow rate, namely a smaller flow rate will result in a higher amount of gas. A better method would be to connect the gas line directly to the GC where the gas will flow through an injection loop. This could not be done as the stack test bench was not located adjacent to the GC. The graphs of the inlet and outlet stack#3 measurements are given in Appendix 7.1.1.6.

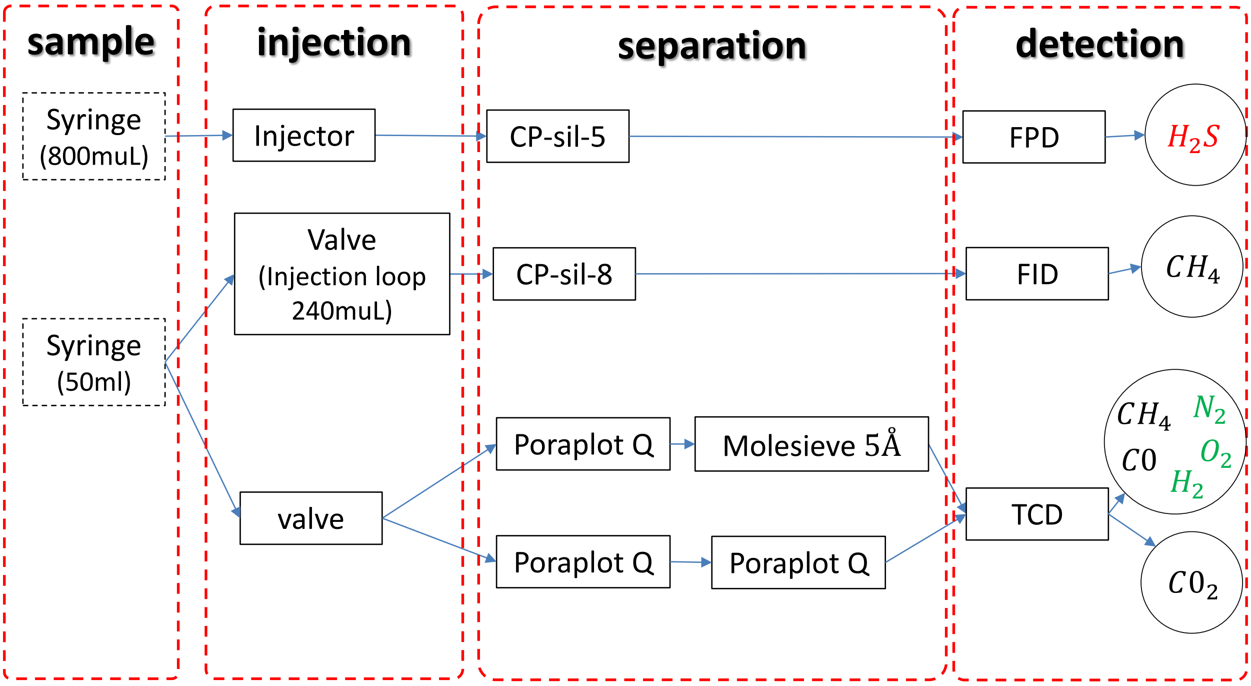

Figure 5: Configuration of the GC enabling the measurement of permananent gases, hydrocarbons and sulfur compounds, including four different separation colomns and three detectors.

This project has received funding from the European Union's Horizon 2020 research and innovation programme under grant agreement No 815284

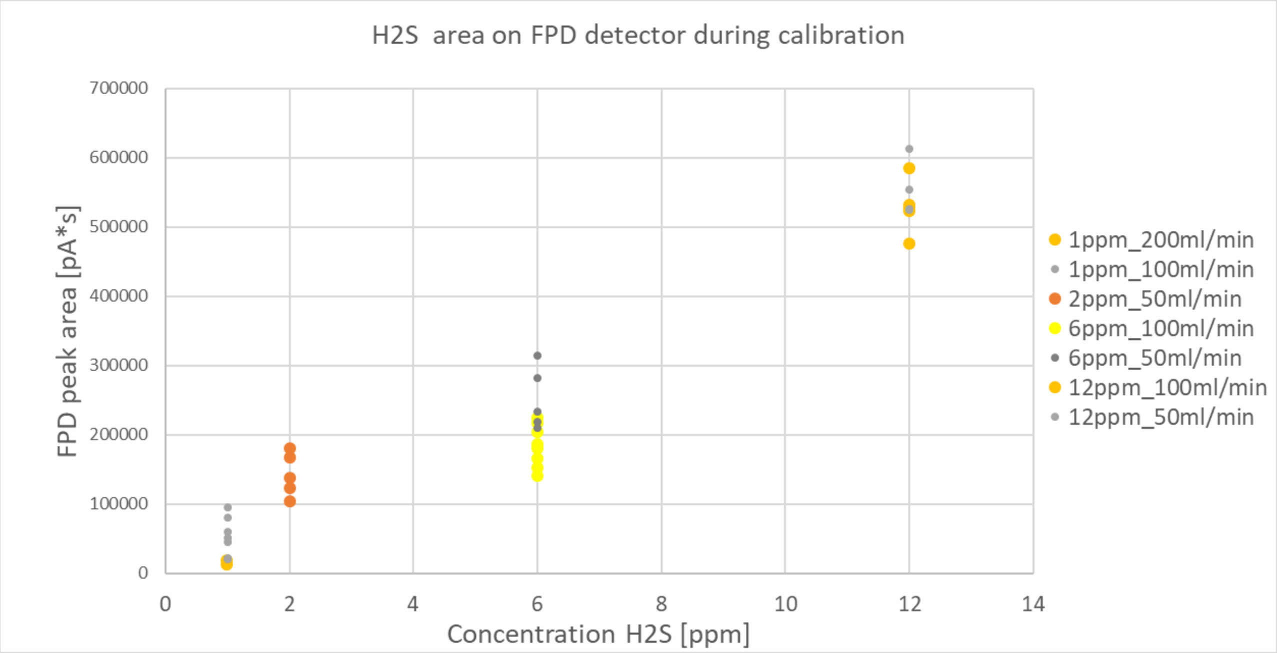

Figure 6: Known flow rate concentration of H_2S in H_2 measured on FPD detector. The gas samples were collected through a septum in the line with a syringe, the sample was manually injected in the GC.

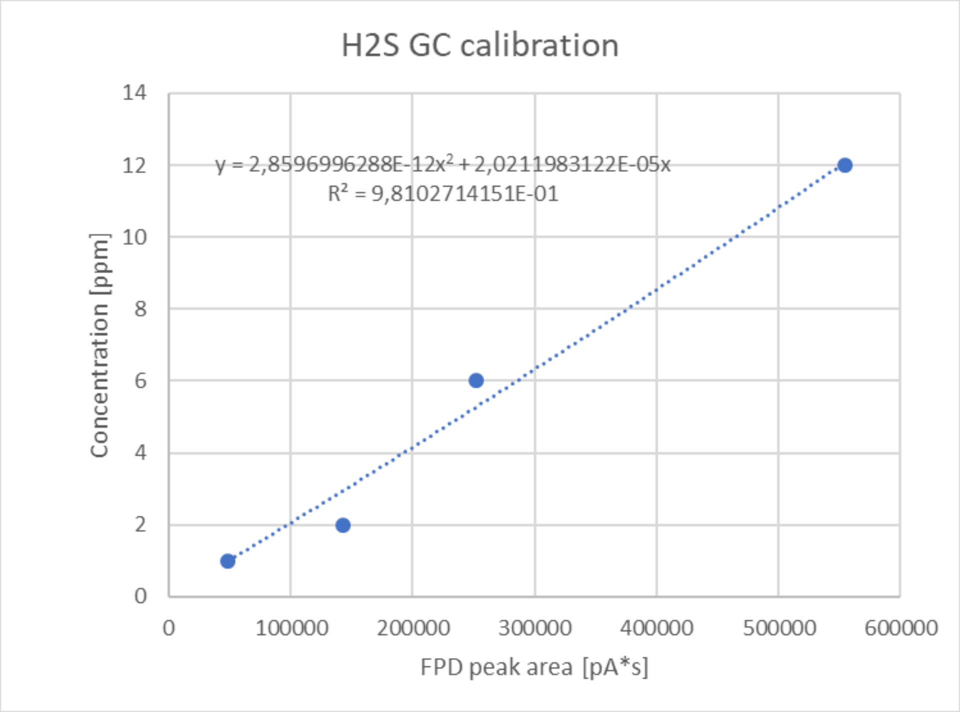

Figure 7: H_2S calibration curve of the FPD detector with the Gas Chromatograph. The mean values of the data from Figure 6 were used.

3.6 EIS, DRT

Electrochemical impedance spectroscopy measurements have been performed with commercial devices from Zahner, i.e. Zennium X connected to an electrical load EL1000, to allow to sink 32 A, instead of only 2 A with the Zennium apparatus only. The perturbation frequency ranged from 100 kHz to 15 mHz where 15 measurements per decade were recorded, with 10 cycles per measurement above 66 Hz and 7 cycles from 66 Hz down to lower frequencies). The perturbation amplitude was set to 1 A for stack#1 (3.1% of the bias) and 2 A for stacks#2 and #3 (6.3% of the bias). The measurement took 1h08 plus 30 min of stabilization before the measurement. Thales software from Zahner was used to smooth the raw data. The smoothed data were compared to the raw data (dots) and as a mismatch was visible at the inflexion point and maximum, the raw data were chosen in the Nyquist and Bode representations.

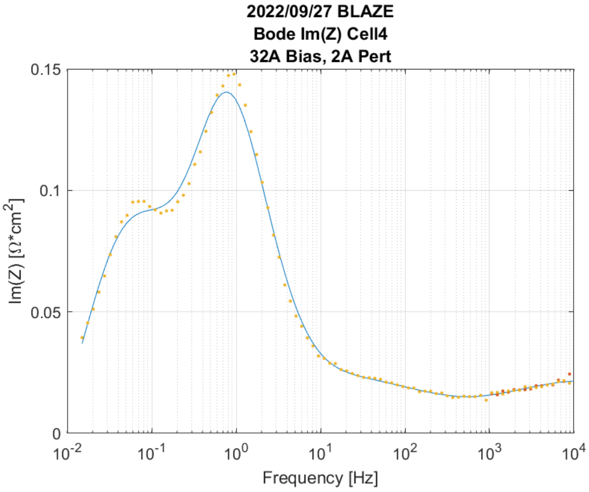

Figure 8: Raw (dots) data in yellow and red. Smoothed data in blue.

The quality of the measurement was checked using the “Z-HIT” tool from Zahner [2]. Figure 9 shows the Z-HIT result applied to the first EIS measurement under reference conditions. The impedance module measurement (in black) and its approximation (in purple) deviate from each other above 10^4 Hz. Thus frequencies higher than 10^4 Hz are not fully reliable.

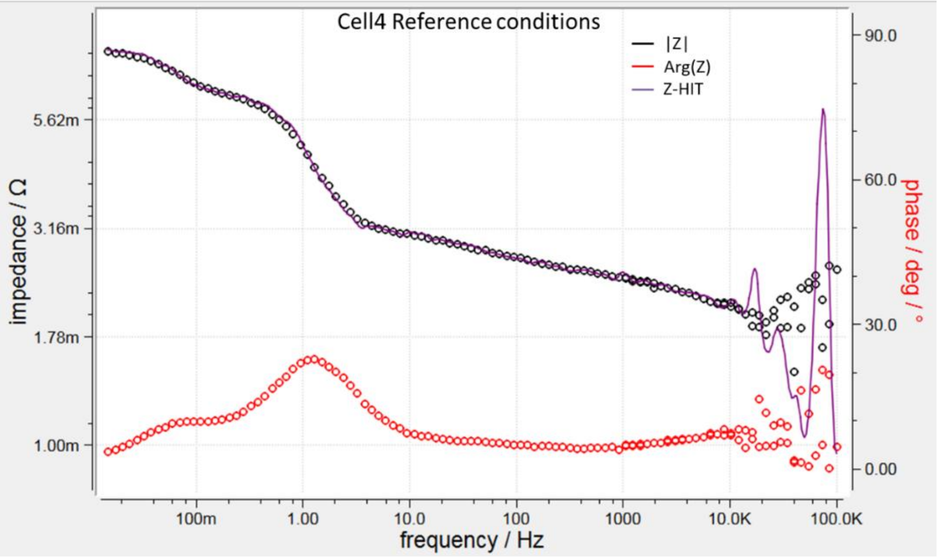

Figure 9: Screenshot of Zahner analysis software. The purple plot is the impedance module evaluated from the phase with the Z-HIT approximation. The approximation and the measured module diverge above 10 kHz.

In addition, the distribution of relaxation times analysis (DRT) was performed to identify processes affected by the contaminant exposure. A MATLAB GUI called DRTtools, based on Tikhonov regularization and developed by researchers from Hong Kong University [3] was used with the parameters listed in Table 3. The DRTtools application is performing a fit prior to the discretization; since its model assumes an imaginary impedance of zero at high frequency (no inductance), the deconvolution is based on the full spectra (up to 100 kHz) of the raw impedance data. Figure 10 shows the influence of the different “Inductance” options in DRTtool: “discard inductive data” will delete all data points with the imaginary of the impedance larger than zero prior to the fit, whereas “Fitting w/o inductance” will fit all data and delete the fitted data with Im(Z) larger than zero. It influences only the high frequency data above 10 kHz, where the Z-HIT test shows inaccuracy. The option “Fitting w/o inductance” was therefore preferred as the result is smoother but it still should be taken with caution. The location and area of the peaks are evaluated with the free Matlab code “peakfits.m” [4].

Table 3: Parameters set in DRTtools

Parameter	**Value**	**Parameter**	**Value**
Discretization method	Gaussian	Regularization parameter	1,E-04
Data used	Combined Re Im	RBF shape control	FWHM coefficient
Inductance	Fitting w/o inductance	FWHM Control	0,5
Regularization derivative	2nd order	Run	Simple run

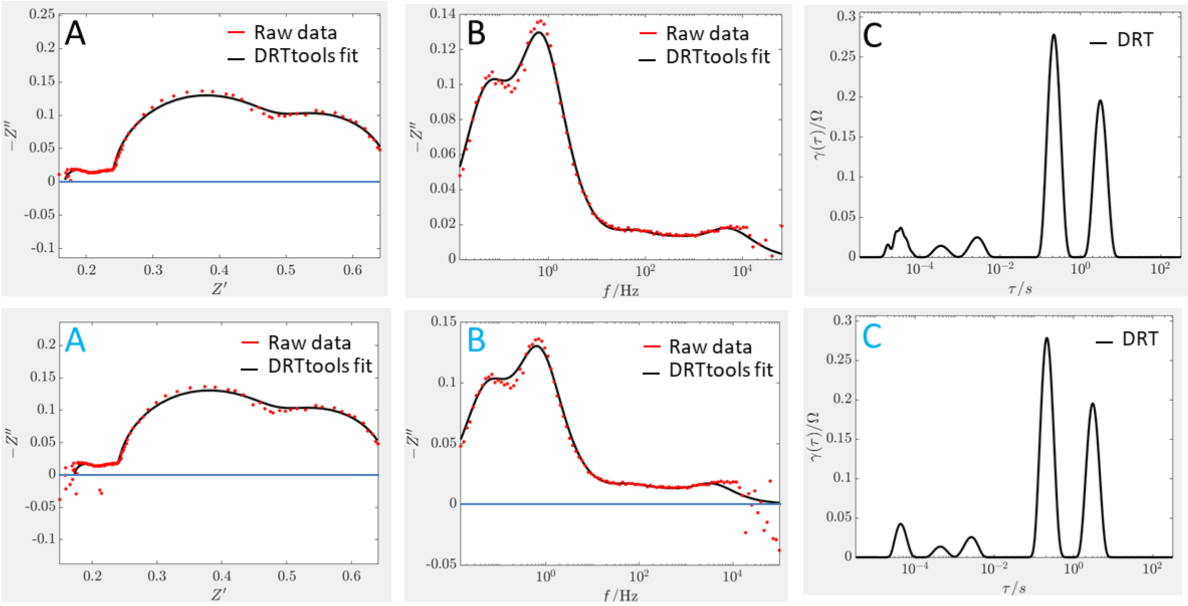

Figure 10: Two ways DRTtools deals with inductance. Top row “Discard inductive data”, bottom row “Fitting w/o inductance”. A: Nyquist plot, B: Bode plot of Im(Z), C: DRT plot.

Concerning the polarization resistance, it was computed from the area under the Bode plot using the Kramers-Kronig relation [5] where $Z''(x)$ is the imaginary part of the impedance and x is the frequency:

$$R_{pol} = \frac{2}{\pi}\int_0^{\infty} \frac{Z''(x)}{x}\,dx$$

The numerical value is obtained in Matlab using the *trapz* function to integrate. This value is compared to the sum of the DRT peaks coming from the interpolation of the function *peakfit*.

The polarisation resistance obtained both ways show a discrepancy due to the inexact fit by DRTtools and *peakfit*. Under dry H_2 (reference conditions), it was estimated that the Rpol from the Bode plot is 485 $m\Omega cm^2$, whereas the sum of the DRT peaks is 504 $m\Omega cm^2$, i.e. 4% of error, which is considered as acceptable. *Peakfit* provides a fast estimate of the areas delimiting the peaks; when peaks are overlapping, an estimate of the gaussian shape of each peak is proposed as visible on the last three peaks in Figure 11.

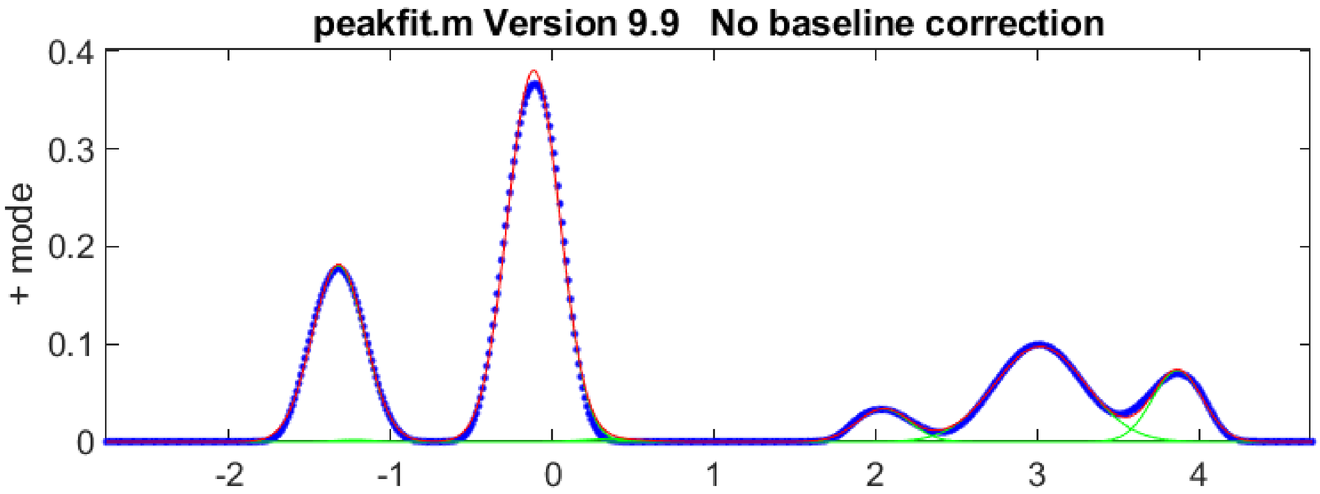

Figure 11: DRT fit from *peakfit* (4 ppm DMS, 400 ppm toluene). Blue: data point from DRT tool. Red: fit from peakfit. Green: Individual peaks contained in the red fit.

4 RESULTS AND DISCUSSION

Three short stacks from SOLIDpower/SolydEra have been tested within Task 3.4. The main results are presented and discussed in this section. There are similarities between the different tests but as the third test was the most complete, the explanations given in the analysis of the third test give also the most complete description, including of observations mentionned for the first 2 stacks.

4.1 Stack 1, 2 and 3 performance summary

Table 4: Initial OCV values of stack 1, 2 and 3 under reference conditions.

	stack #	U1 bottom	U2	U3	U4	U5	U6 top	mean
OCV [V]	1	1,226	1,221	1,225	1,225	1,217	1,210	1,22
	2	1,201	1,200	1,194	1,203	1,194	1,199	1,20
	3	1,224	1,227	1,224	1,215	1,226	1,225	1,22

Table 5: Efficiencies of stack 1, 2 and 3 under dry hydrogen (reference conditions)

Reference conditions / Dry hydrogen						
stack #	**Time**	**U stack [V]**	**I stack [A]**	**Pelec [W]**	**Eff HHV [%]**	**Eff LHV [%]**
1	22h	4,84	33	159,9	43,5	51,4
2	276h	4,78	33	157,6	42,9	50,7
3	188h	4,76	33	157,0	42,7	50,5

Table 6: Efficiencies of stack 1, 2 and 3 under synthetic woodgas conditions (SG2)

Syngas conditions (SG2)						
stack #	**Time**	**U stack [V]**	**I stack [A]**	**Pelec [W]**	**Eff HHV [%]**	**Eff LHV [%]**
1	800h	4,69	32,10	150,6	41,98	49,36
2	4432h	4,81	32,05	154,1	42,95	50,49
3	690h	4,75	32,00	152,1	42,40	49,84

4.2 Stack#1

4.2.1 Baseline

Figure 12 gives an overview of the test with the first stack, which lasted more than 9000 h. As can be seen in the figure, the cell voltages were initially noisy due to the steam generation. Optimal operating conditions were found after 3000 h. From there on, the cell voltages were stable except for cell 6, which had degraded from the start. The average degradation rates ranged between -3.4 mV/kh (-0.4%/kh) for cell 5 and -26 mV/kh (-3.3%/kh) for cell 6. Electrochemical impedance spectroscopy (EIS) measurements revealed that cell 6 differed from the other 5 cells by larger ohmic losses (cf. Figure 13A), whereas the imaginary part of the impedance, which reflects the polarisation losses, are similar (cf.Figure 13B). This indicates that RU 6 suffered from a contact issue. Looking at the time evolution of cell 3 and 4 during the last 3000 h (cf. Figure 14), it can be observed that the degradation is also mainly ohmic, as the polarisation resistance apparent in the imaginary Bode plot scarcely changes over time (cf. Figure 14B).

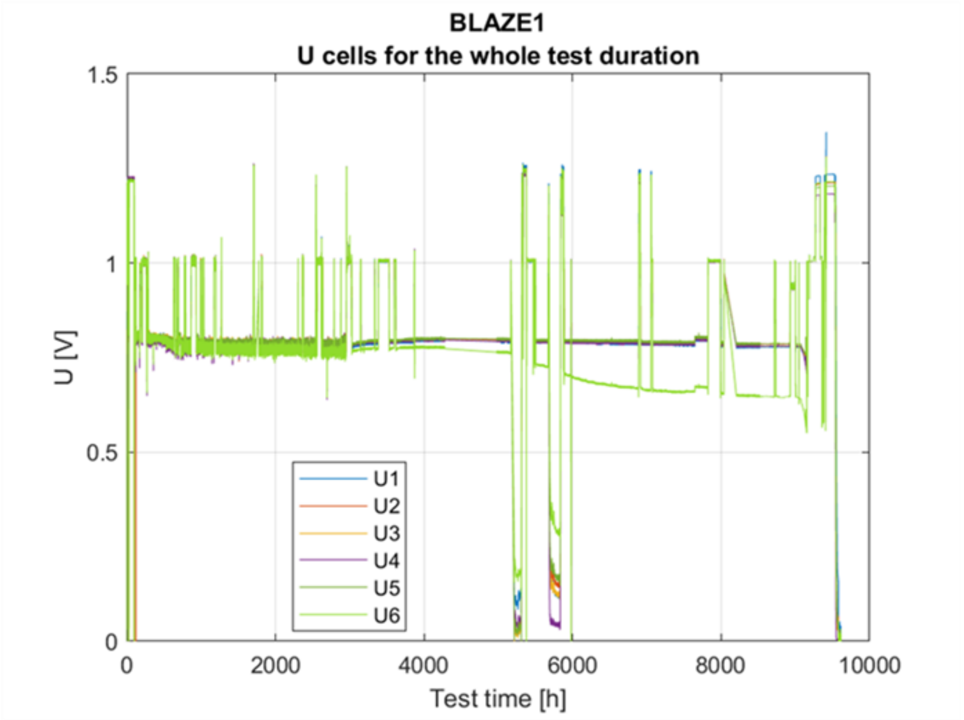

Figure 12: Overview of the short stack#1 test (750°C air outlet, 32 NL/min air, 69% H_2, 11% CO_2, 2% CH_4, 18% H_2O) polarized at 32A.

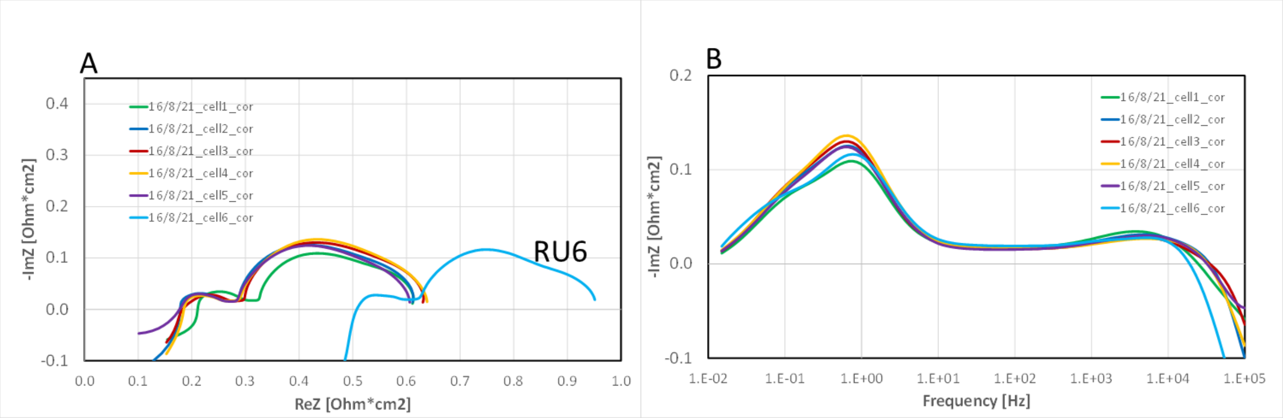

Figure 13: Nyquist (A) and ImZ Bode plot (B) plots of EIS data measured at 32 A bias (100 kHz – 15 mHz, 1A perturbation) with synthetic woodgas (69% H_2, 11% CO_2, 2% CH_4, 18% H_2O)

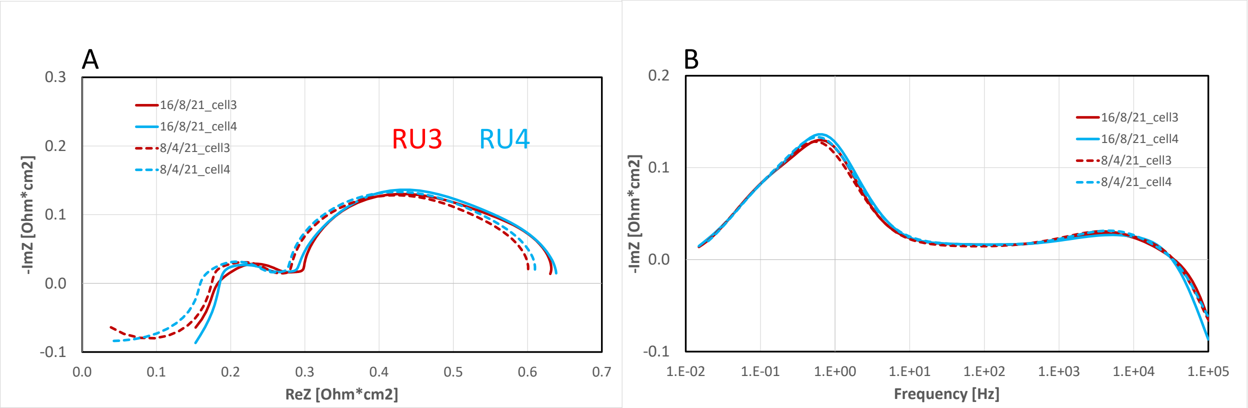

Figure 14: Nyquist (A) and ImZ Bode plot (B) plots of the EIS data measured at 32 A bias (100 kHz-15 mHz, 1 A perturbation) with synthetic woodgas (69% H_2, 11% CO_2, 2% CH_4, 18% H_2O) for RU 3 and 4 during the last 3000h.

4.2.2 Preliminary test of contamination

At the end of the test, impurity injection tests were made, to check the methodology. The performance loss due to sulfur, visible in Figure 15, appeared 70 h after the contamination start. DMS concentration began at 0.5 ppm for 44 h, then 2.5 ppm for 6 h, 5 ppm for 15 h and again 0.5 ppm for 5h more. The degradation rate was more prominent for cells 3 and 6 that lost 90 mV in 80 h. The voltage loss of the other cells was 30 mV in 80 h. EIS measurements were performed before and after the sulfur exposure without reducing the polarisation, thanks to the spectrometer adapted for high current. As expected, the high frequency part of the spectra was mainly affected, indicating that the sulfur contamination reduces the activity of the triple phase boundary of the fuel electrode (cf. Figure 16). This observation is consistent with literature. However, the exact concentration of sulfur injected was not certain at this point because of the inaccurate GC calibration.

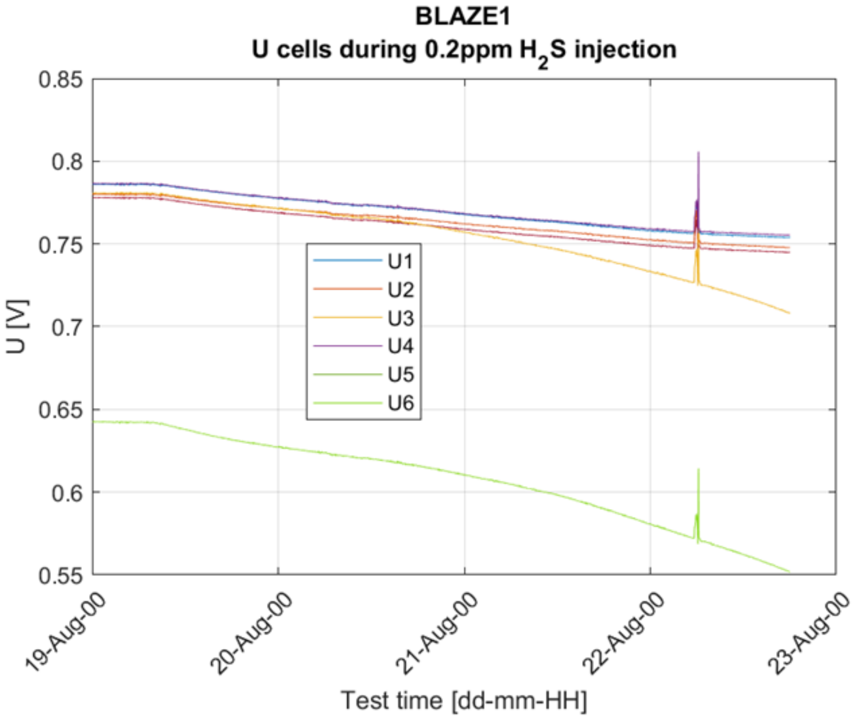

Figure 15: Evolution of cell voltage consecutive to the first injection of a sulfur impurity. Conditions as in Figure 12

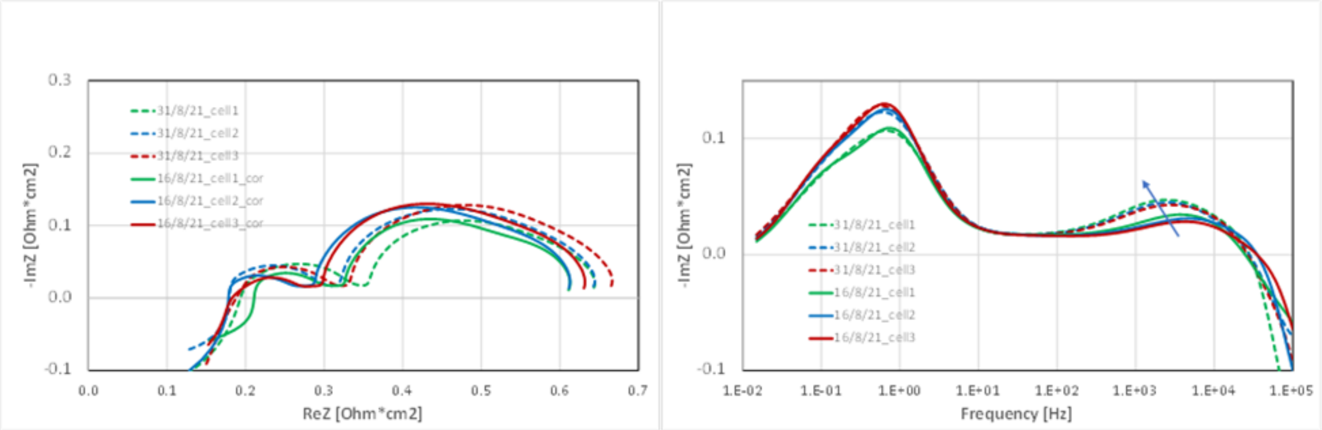

Figure 16: Electrochemical impedance spectra for the first 3 cells of the short stack#1 measured at the same conditions as Figure 12, before and after exposure to sulfur. Left: Nyquist plot; Right: imaginary Bode plot. The arrow indicates the increase of polarisation resistance at high frequency consecutive to the sulfur exposure. (32 A bias, 100 kHz – 15 mHz, 1A perturbation)

4.3 Stack#2

4.3.1 Baseline

Figure 17 gives the full overview of the short stack#2 test history. The stack was operated >7000 h prior to injecting impurites, of which ~4000 h under polarisation (considering a break between 2100 and 3900 h and the 1200 h of OCV starting from 6000 h). Because of an issue with the test bench, the stack experienced 6 unplanned shut-downs. The aforementioned break was used to investigate the computer hardware without improvement, the root cause was found during the third stack test, the phase control relay was found to be too sensitive. After the 6th emergency shut-down, the cells, which had been operating stably before that, started to degrade significantly. Except for RU 4 and 6, which showed strong degradation of -48.6 mV/kh and -56.3 mV/kh respectively, suggesting a stronger impact of the shut-down, the other RU showed a mean degradation of -5.8 mV/kh with a minimum value of -4.9 mV/kh for cell 1 and a maximum value of 6.8 mV/kh for cell 2. These voltage degradation rates prior to the injection phase are taken as reference and are regrouped in Table 7.

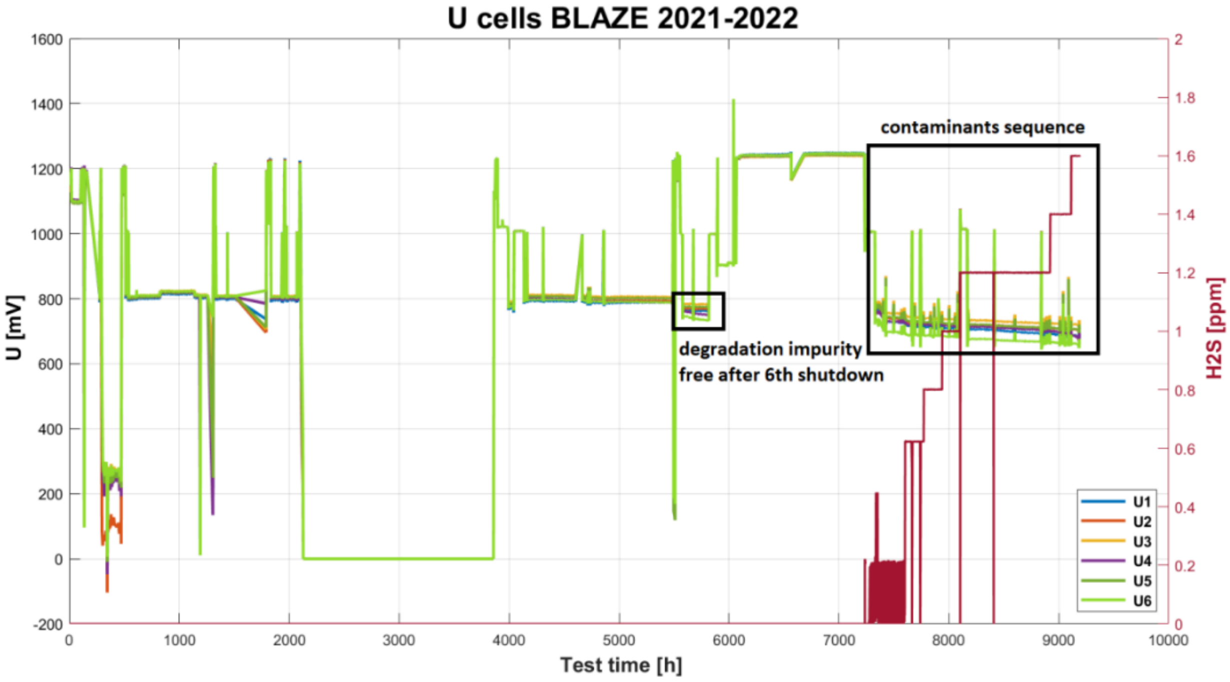

Figure 17: Overview of the stack#2 test, showing multiple unintended emergency-stops. Injection of impurities started after 7000h.

Table 7: Degradation rates for the individual repeating units after the 6th e-stop but prior to the injection of impurities.

Cell number	1	2	3	4	5	6
Degradation [mV/kh]	4.92	6.85	5.00	48.64(!)	6.28	56.35(!)

To be noted also is that the stack#2 was set to OCV for 1000 hours between the impurity free degradation sequence and the contaminant injection. The stack was polarized back on 17.01.2022 to start with the injection on 18.01.2022.

4.3.2 Contamination

A zoom of the stack voltages (left Y-axis) and the impurity levels (riht Y-axis) during the contaminant injection sequence is given in Figure 18. The lowest and first contaminant flow (H_2S level of 0.2 ppm at 7400 h) shows very noisy values, oscillating between the set value and zero. This is because the set flow was close to the minimum opening value of the mass flow controller. A delay of 25 h preceded the start of the voltage loss. Unfortunately, the H_2S level of 0.4 ppm was skipped by mistake, therefore the investigated contaminant levels were 0.2, 0.6, 0.8, 1.0, 1.2, 1.4 and 1.6 ppm. During the last contaminant level, the voltages of RU 2, 3 and 5 were still above 0.7 V, which is the redox potential of the nickel oxidation reaction, and thus pursuing the exposition was still considered relevant. After 9280 h, RU 2 and RU 5 voltages went below 0.7 V and the test was automatically stopped 3 days laer as cell 4 reached the minimal set voltage value of 0.55 V. This low value was chosen to allow the test campaign to continue despite RU 4 was dropping.

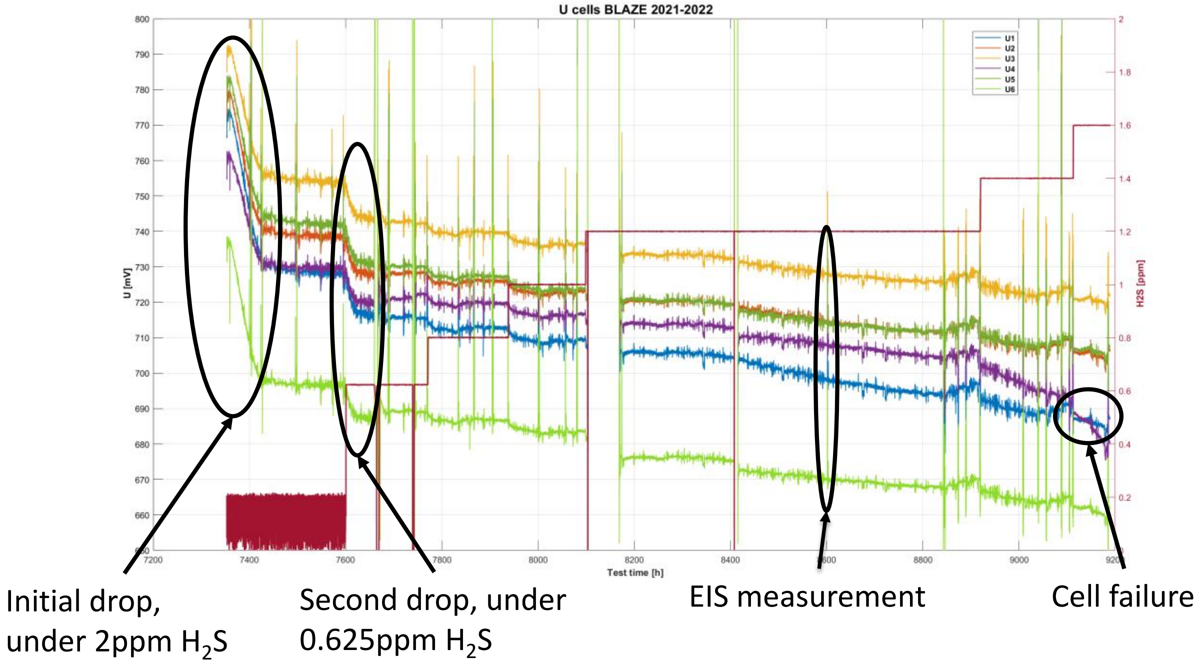

Figure 18: overview of the impurities injection sequences, showing the stepwise increase of H_2S content.

Investigation of this failure revealed that the point at which cell 4 (in green) starts to drop steeply, coincides with the moment that the air inlet pressure exceeded that of the fuel (cf. Figure 19). The sudden increase of the air inlet pressure was due to a malfunctioning of the MFC controlling the air stream, increasing in an uncontrolled manner the air flow and thereby the pressure drop on the air side. At some point, the pressure of the air compartment exceeded that of the fuel compartment and air leaked in the anode, presumably through a pinhole or microcrack, reoxidizing the Ni catalyst and inducing cracks.

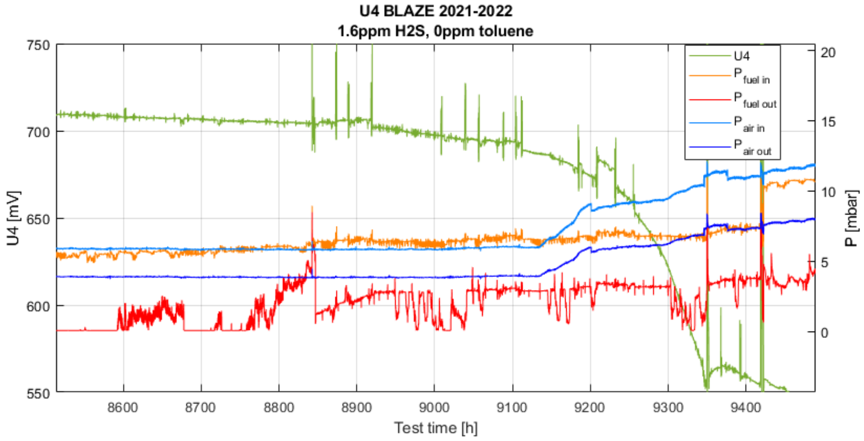

Figure 19: Gradual increase of the air flow that led to the final failure of RU 4.

As a consequence of this failure, the last measured H_2S level has been disregarded and, in the end, only 6 levels were investigated, namely, 0.2, 0.6, 0.8, 1.0, 1.2 and 1.4 ppm. Furthermore, the level of 1.2 ppm of H_2S was kept for a longer exposure period in comparison to the other levels. The reason was the occurrence of a gas alarm in the lab and a power cut (responsible for respectively the first and second points at OCV) which delayed the injection sequence for toluene. Figure 20 gives a more detailed overview of the cell voltages behaviour during the first injection level of the contaminants. For the sake of clarity, the voltages before the drop and at the start of the stable degradation have been highlighted in black. The voltage first decreases rapidly (voltage drop) before stabilising to a new steady degradation rate. All voltage drops consecutive to the change in S-contaminant levels are summarised in Table 8 and Table 9, along with the corresponding degradation rates. The voltage drop is maximum after the first step (0.2 ppm) but then strongly reduces. This behaviour is consistent with observations reported in literature [6] with similar cells and explained by the gradual deactivation of electrochemically active sites by the adsorption of sulfur [7] on Ni. Hansen has shown that S-adsorption follows a Temkin-like isotherm and that the performance loss is linearly proportional to surface coverage. This is shown by plotting the cumulative performance drop expressed in % against the calculated surface coverage (cf. Figure 21). The adsorbed sulfur coverage (θ_S) can be calculated using equation (1), where T is the operating temperature of the stack (1023K) and H_2S/H_2 stands for the ratio between the molar fraction of H_2S and that of hydrogen.

$$\theta_s = 1.45 - 9.53 \cdot 10^{-5}T + 4.17 \cdot 10^{-5}T \ln\left(\frac{\mathrm{H_2S}}{\mathrm{H_2}}\right) \quad (1)$$

Most of the coverage occurs during the first step and reaches 70% at 0.2 ppm of H_2S. The further six-fold increase of H_2S partial pressure only results in 80% surface coverage.

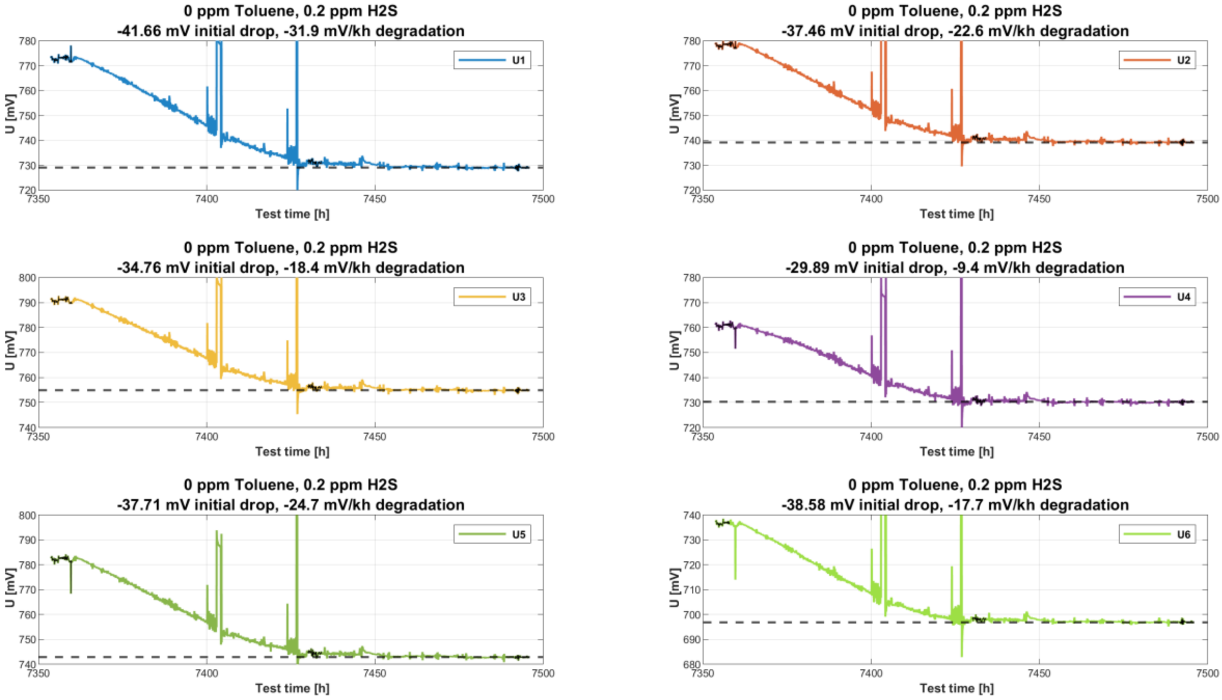

Figure 20: Cell voltage drop consecutive to exposure to 0.2 ppm H_2S. Other conditions similar to Figure 12.

Table 8: Summary table of the initial voltage drops and consecutive degradation rate following the injection of different levels of sulfur.

	Voltage drop [mV]							**Degradation rate [mV/kh]**						
H2S [ppm]	**Cell1**	**Cell2**	**Cell3**	**Cell4**	**Cell5**	**Cell6**	**average**	**Cell1**	**Cell2**	**Cell3**	**Cell4**	**Cell5**	**Cell6**	**average**
0.2	41.7	37.5	34.8	29.9	37.7	38.6	**36.7**	31.9	22.6	18.4	9.4	24.7	17.7	**20.8**
0.625	9.6	8.6	8.3	8.3	9.0	8.3	**8.7**	36.7	28.7	30.4	19.8	29.7	19.8	**27.5**
0.8	1.7	1.5	1.4	1.5	1.5	1.4	**1.5**	20.0	17.3	18.4	18.9	19.2	17.9	**18.6**
1	2.1	1.9	1.9	1.9	2.7	1.7	**2.0**	22.8	20.4	21.5	21.9	18.1	21.9	**21.1**
1.2	2.6	4.6	2.4	1.9	2.0	6.7	**3.4**	31.6	40.9	27.9	27.9	20.5	31.6	**30.1**
1.4	2.4	2.0	1.8	1.8	1.8	1.9	**2.0**	31.6	26.6	22.3	61.4	22.7	25.0	**31.6**

Table 9: Cumulative voltage drop consecutive to the different levels of H_2S exposure expressed in mV (shaded cells) and % of the reference cell voltage used for the sulfur coverage calculation.

H2S [ppm]	**RU1**	**RU2**	**RU3**	**RU4**	**RU5**	**RU6**	**RU1**	**RU2**	**RU3**	**RU4**	**RU5**	**RU6**
0,2	41,7	37,5	34,8	29,9	37,7	38,6	5,4%	4,8%	4,4%	3,9%	4,8%	5,2%
0,625	51,2	46,0	43,1	38,1	46,7	46,9	6,6%	5,9%	5,5%	5,0%	6,0%	6,3%
0,8	52,9	47,5	44,5	39,6	48,3	48,3	6,8%	6,1%	5,6%	5,2%	6,2%	6,5%
1	55,0	49,5	46,4	41,5	50,9	50,0	7,1%	6,3%	5,9%	5,4%	6,5%	6,7%
1,2	57,6	54,1	48,8	43,4	52,9	56,7	7,5%	6,9%	6,2%	5,7%	6,8%	7,6%
1,4	59,9	56,1	50,6	45,2	54,7	58,5	7,8%	7,2%	6,4%	5,9%	7,0%	7,8%

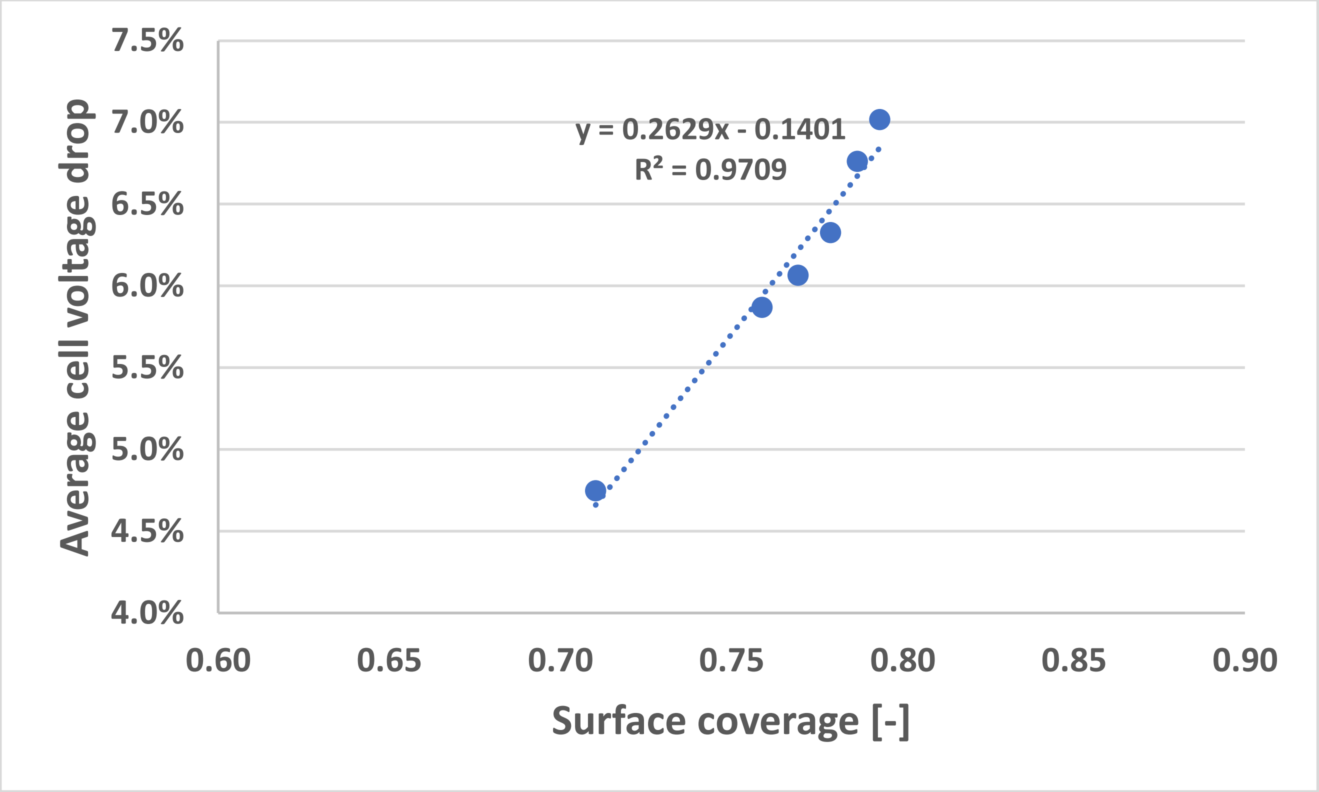

Figure 21: Cumulative voltage drop consecutive to exposure to different levels of H_2S (cf. Table 9) as a function of surface coverage of Ni by sulfur assuming Temkin-like isotherm.

Figure 22 shows electrochemical impedance spectra measured consecutively on cell 2 during the 0.2 ppm H_2S poisoning. As previously observed with short stack#1, the S-poisoning affects solely the polarisation resistance of the cell, since the ohmic resistance, given by the intercept with the real axis at high frequency in the Nyquist plot (left of Figure 22A), remains constant over time. The frequency regions impacted by S-poisoning are best seen in the imaginary Bode plot (Figure 22B). A major increase of the peak around 1 kHz is observed along with that at 1 Hz. This behaviour is consistent with literature. The high frequency peak is attributed to charge transfer at the anode/electrolyte interface. Sulfur is known to adsorb strongly on the nickel catalyst in the anode, and thereby to deactivate the electrochemically active sites. The low frequency peak is associated with the fuel conversion impedance, which is sensitive to changes in gas composition within the anode. Here again, by adsorbing on the nickel particles, sulfur deactivates the catalytical properties of the anode, hindering the reverse water-gas-shift reaction, resulting in a hydrogen richer mixture at the beginning of the anode channels. As the moisture ratio of the fuel outlet over the fuel inlet is higher, the conversion peak is bigger. The internal reforming of methane should also be limited by the sulfur coverage, this will be addressed in the gas analysis of the stack#3.

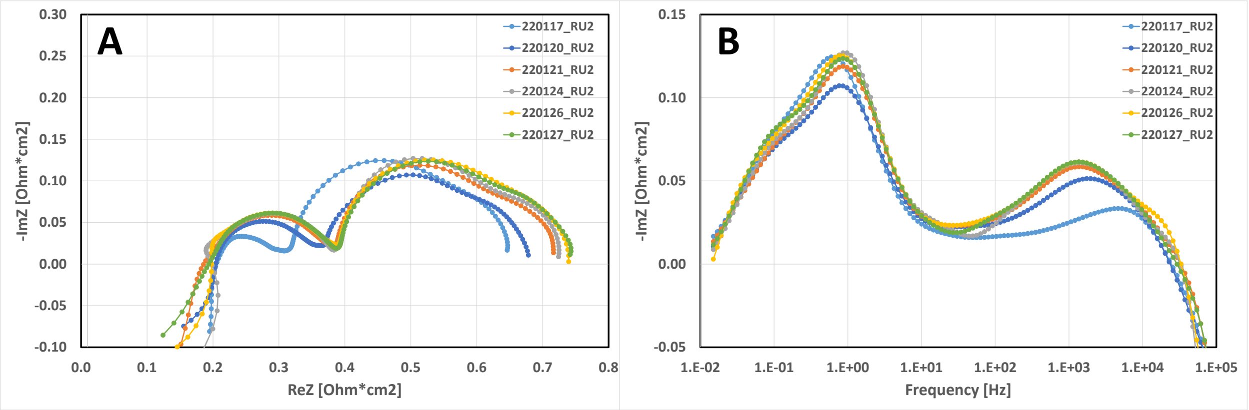

Figure 22: Time evolution of the Nyquist (A) and imaginary Bode (B) plots for RU2 during exposure to 0.2 ppm of H_2S.

For each sulfur level, a triple step of toluene exposure was superimposed, as illustrated in Figure 23. Contrarily to sulfur, toluene did not impact the performance of the cells in the presence of sulfur, as apparent in this figure for 20-60 ppm toluene addition, but also for values up to 180 ppm toluene injected later on in this test.

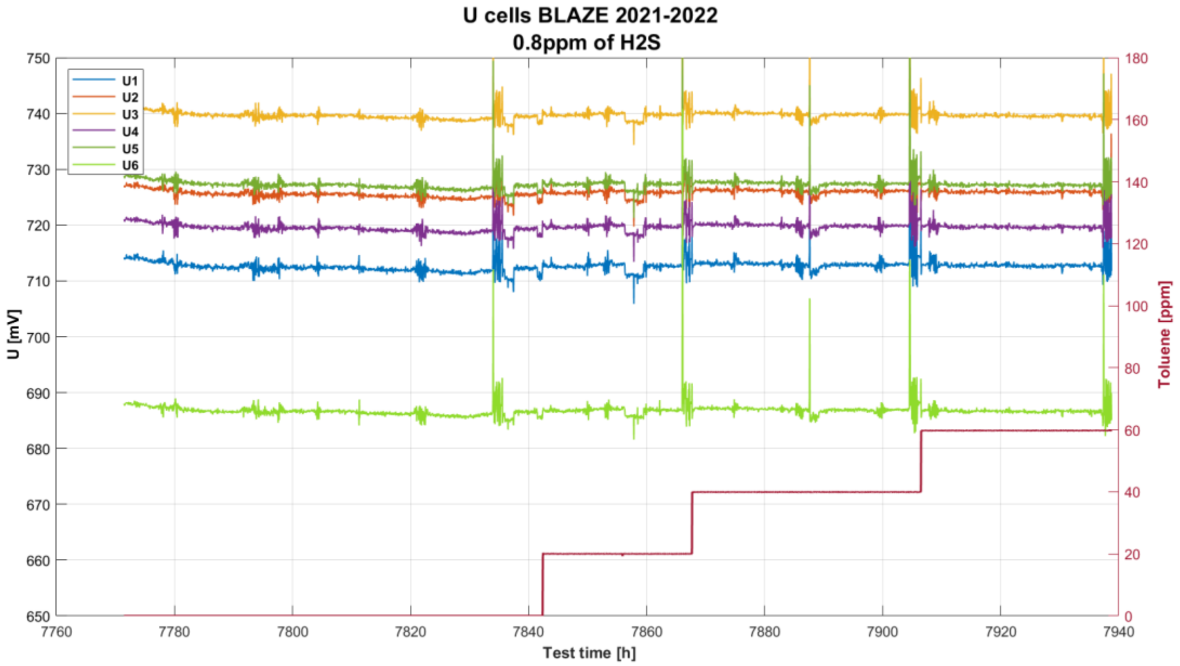

Figure 23: Evolution of the cell voltages consecutive to the exposure to increasing levels of toluene (0, 20, 40 and 60 ppm) in addition to 0.8 ppm of H_2S injection.

4.4 Stack#3

The overall evolution of the cell voltages is plotted in Figure 24. The stack ran for 7000 h and experienced 3 emergency stops during the first 1300 h, before the exposure to impurities. A phase control relay was found too sensitive, already disturbing the previous tests, after which it was set to a similar value as in other test benches. Beginning of October 2022, stack#3 was tested in reference conditions (60% H_2, 40% N_2), and then with the baseline gas mixture for several weeks. From the end of November 2022 to the end of

February 2023, the stack was exposed to DMS and toluene, allowing recovery until June 2023 when finally HCl injection was performed.

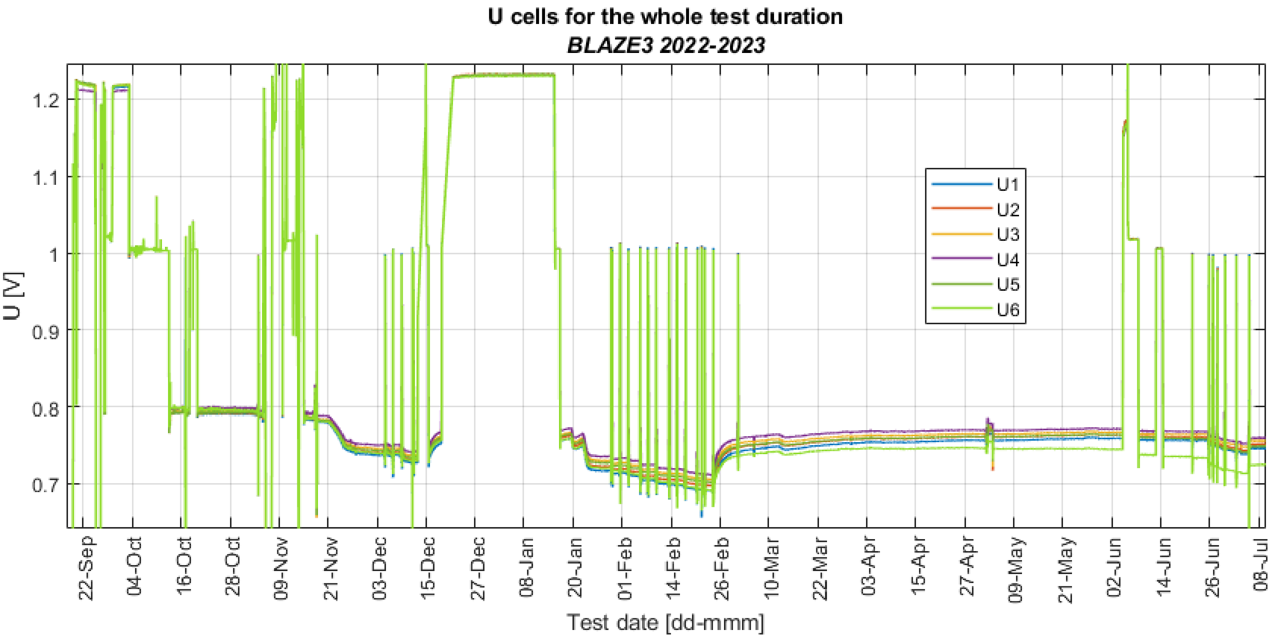

Figure 24: Overview of short stack#3 test (750°C air outlet, 32 NL/min air, 69% H_2, 11% CO_2, 2% CH_4, 18% H_2O) polarized at 32 A.

4.4.1 Reference conditions vs synthetic woodgas

An initial EIS measurement was performed to determine the stack health under reference conditions (dry H_2). According to the Nyquist plot of

Figure 25, all repeating units show a similar ohmic resistance. It is noticeable that cells 2, 3 and 5 show a larger polarization resistance (R_{pol}), confirmed on the Bode plot, where the polarization resistance computed from the Kramers-Krönig relation shows a value of 535 $m\Omega cm^2$ for cell2, 494 $m\Omega cm^2$ for cell 5 and 491 $m\Omega cm^2$ for cell 3. Cell 1 has the smallest R_{pol}, 13% smaller than cell 2.

Then the impact of the gas feed composition was investigated. A V-I curve under dry H_2 and the two different wood gas compositions was already compared in Figure 4. Hereafter, EIS measurements are compared between dry H_2 (reference conditions) and SG2. The ohmic resistance stays similar for both cases. The small variation in polarisation resistance is better seen in the DRT plot of Figure 26.

The higher polarization resistance of the dry mixture comes mainly from the 2nd peak, known to be related to the level of gas conversion in the anode [8]. The fuel utilization is 77% and the bias 32 A in both cases. In the dry condition, the amount of steam went from very low (~0.1%) to 46.5% along the fuel channels, whereas in the SG2 mixture, it contains already 18% of steam at the inlet, leading to a lower conversion resistance. The higher total flow rate used in dry conditions lowers the conversion resistance compared to a smaller flow rate. The difference in area specific resistance of P2 would have been more important with the same total flow rate in both conditions. P5 is also larger with syngas [9].

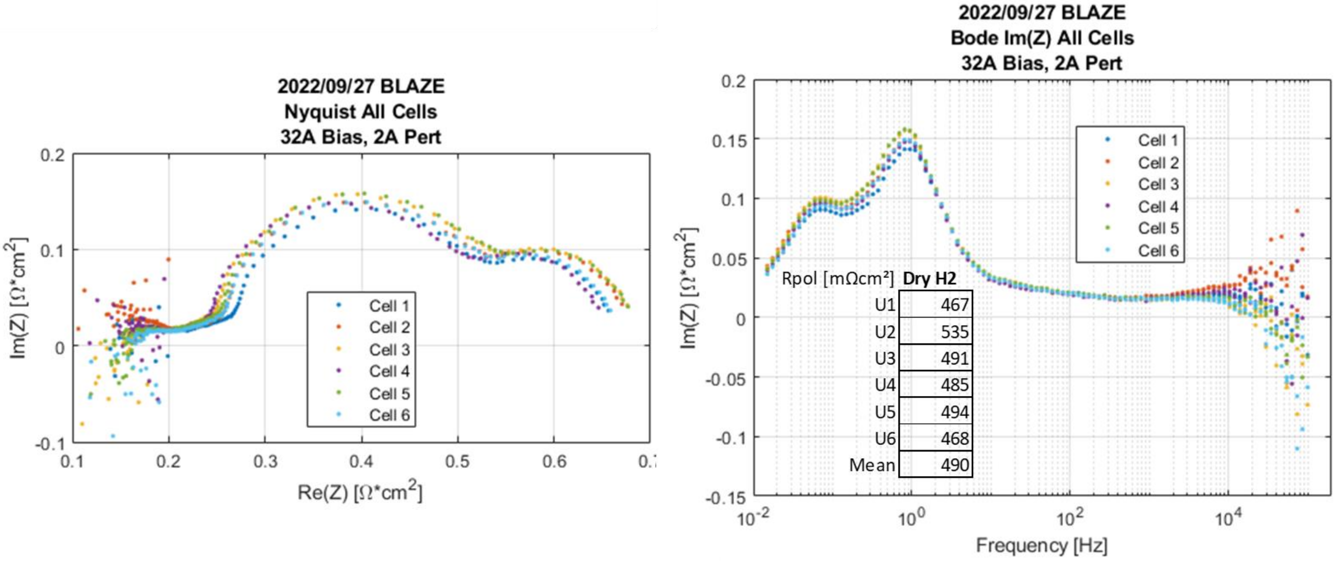

Rpol [mΩcm²]	Dry H2
U1	467
U2	535
U3	491
U4	485
U5	494
U6	468
Mean	490

Figure 25: Nyquist (left) and Bode Im(Z) (right) at reference conditions. 60% H_2, 40% N_2, 6 Nml/min/cm^2

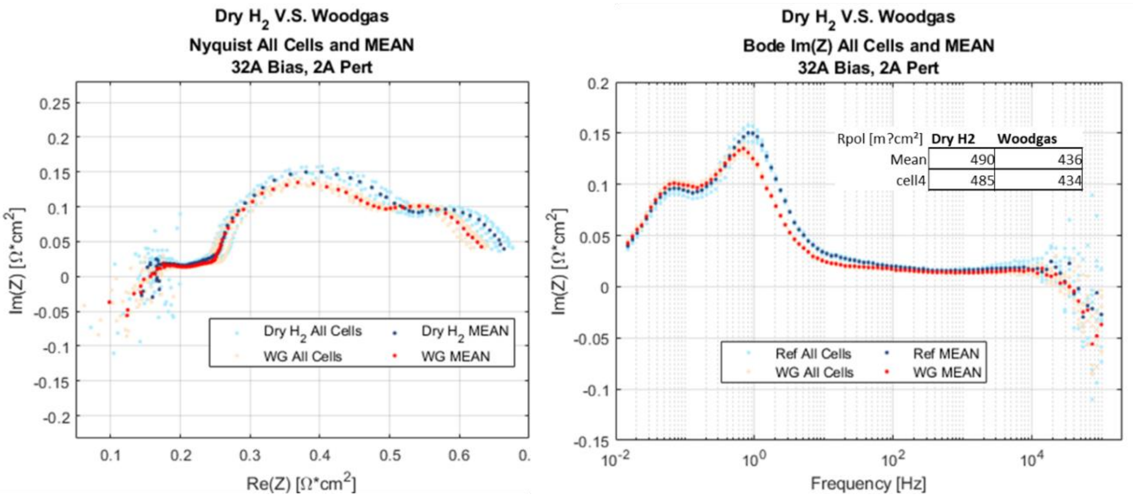

Rpol [m?cm²]	Dry H2	Woodgas
Mean	490	436
cell4	485	434

Figure 26: Nyquist (left) and Bode Im(Z) (right) under dry H_2 (60% H_2, 40% N_2, 6 Nml/min/cm^2) and wood syngas#2 (69% H_2, 11% CO_2, 2% CH_4, 18% H_2O, 4.7 Nml/min/cm^2) cut at 10^4 Hz. The polarization resistance is estimated from the area under the Bode Plot (full spectrum) according to the Kramers-Kronig relation [5].

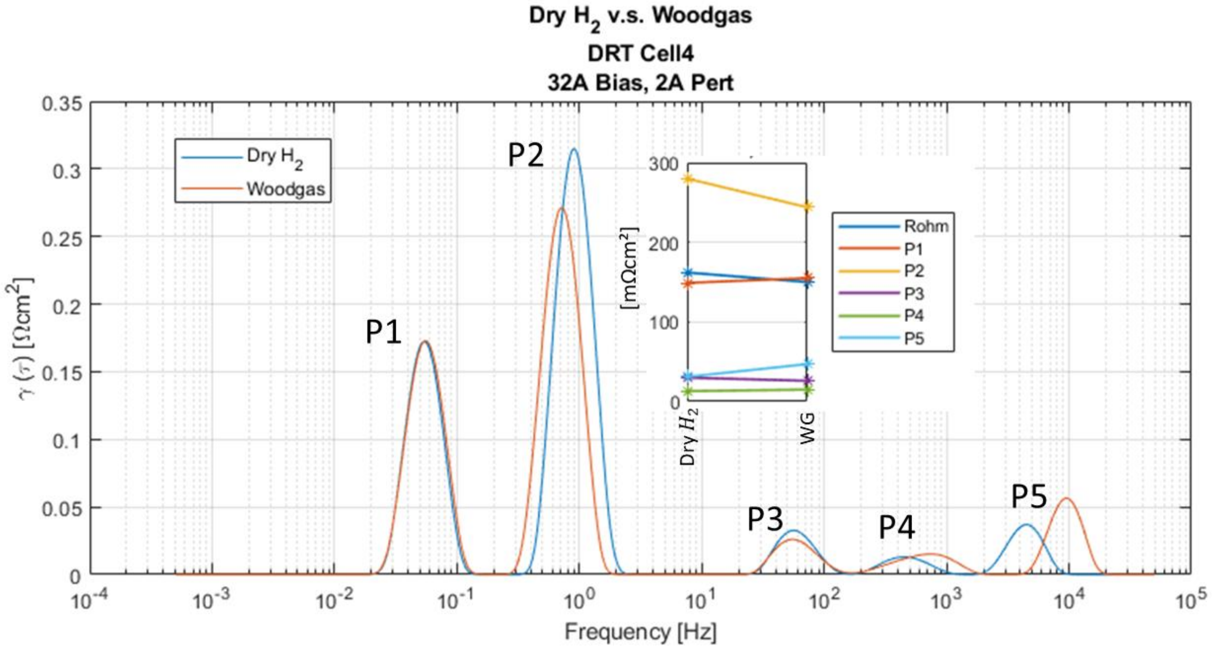

Figure 27: RU4 DRT under dry H_2 (60% H_2, 40% N_2, 6 Nml/min/cm^2) and wood syngas#2 (69% H_2, 11% CO_2, 2% CH_4, 18% H_2O, 4.7 Nml/min/cm^2). Peak areas are displayed on the small chart (computed with peakfit).

Table 10: Detailed peak areas under dry H_2 (60% H_2, 40% N_2, 6 Nml/min/cm^2) and wood syngas#2 (69% H_2, 11% CO_2, 2% CH_4, 18% H_2O, 4.7 Nml/min/cm^2). The polarization resistance is retrieved from the peaks sum. The ohmic resistance is estimated from the Nyquist plot.

[mΩcm²]	**Dry H2**	**Woodgas**
Rohm	*150*	*150*
P1	149	155
P2	280	244
P3	30	26
P4	13	15
P5	31	47
Rpol	*504*	*487*
Rpol Bode	*485*	*434*
error [%]	*4*	*12*

4.4.2 Baseline

The stack ran 570 h in BLAZE syngas conditions plus 2 days of interruption caused by an emergency-stop where the air temperature reached a minimum of 645°C, followed by a pump issue. A shortage of CO_2 occurred 530 h after the baseline test had started. The end V-I curve was recorded after 2 e-stops that led to the complete cooldown of the stack. These events are reported in Figure 28 where the cell potentials and the applied current are represented during the baseline operation. RU6, located at the top of the SOFC, exhibits the best performance at the start of the baseline. During the first 100 h, a slight increase of voltage is visible for all repeating units (1 mV for RU6 and 1.7 mV for RU5). After the E-stop, RU6 experienced a greater degradation than the others, namely 1.8%/kh, whereas RU5, which started with the worst potential, shows the least degradation with 0.7%/kh. Actually, RU5 potential only decreased after the two thermal cycles due to the 2 E-Stops. The cell degradation rates are presented in Table 11.

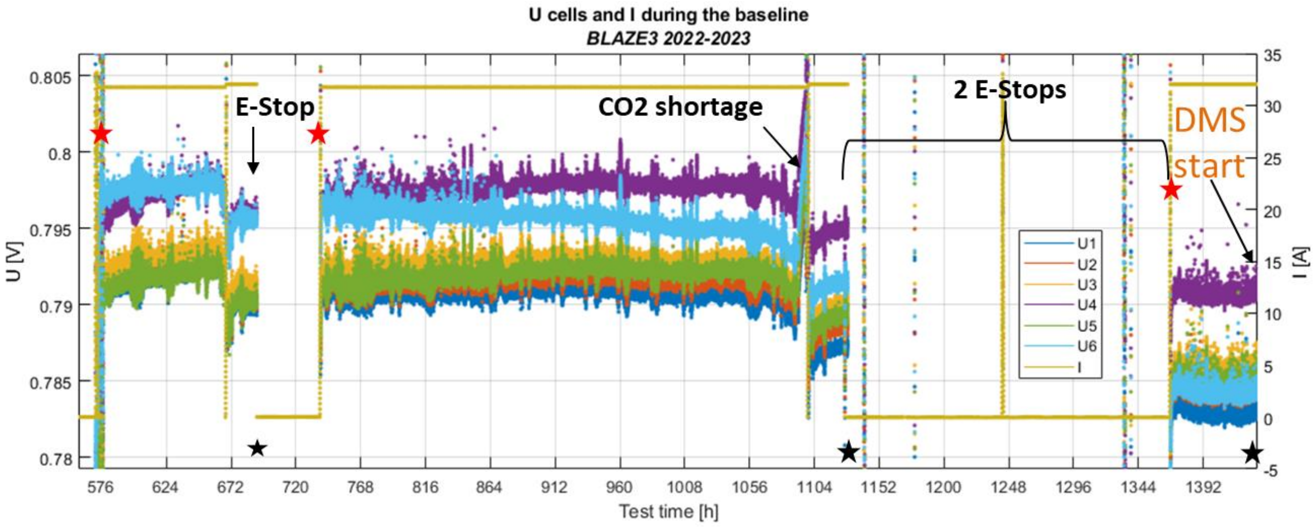

Figure 28: 576h baseline test under BLAZE conditions (without stops). The active load shows an offset of 0.3 A that has been considered only after 672 h until the E-stop, after 1104 h until the E-stop and for the last section. The 3 red stars refer to V-I measurements and the black stars denote where the degradation is computed. EIS is also measured at the beginning (first red star) and end of the baseline (at 1436 h). The air outlet temperature, during the polarization, ranged from 755.9°C to 756.3°C.

Table 11: RU voltages at 32 A during the baseline test. The black stars refer to the time indicated in Figure 28. One E-Stop happens before 1130 h and 2 E-Stops after. The degradation is computed from the first and last black star. Red and green boxes shows best and worst efficient RU.

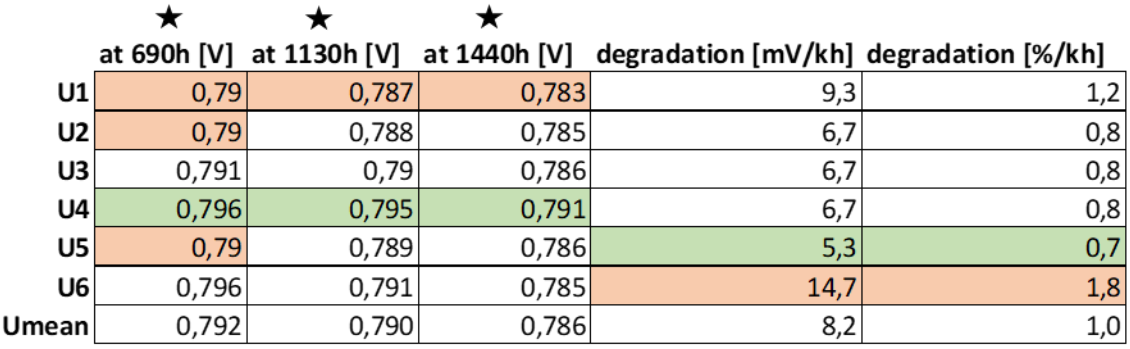

	★	★	★		
	at 690h [V]	**at 1130h [V]**	**at 1440h [V]**	**degradation [mV/kh]**	**degradation [%/kh]**
U1	0,79	0,787	0,783	9,3	1,2
U2	0,79	0,788	0,785	6,7	0,8
U3	0,791	0,79	0,786	6,7	0,8
U4	0,796	0,795	0,791	6,7	0,8
U5	0,79	0,789	0,786	5,3	0,7
U6	0,796	0,791	0,785	14,7	1,8
Umean	0,792	0,790	0,786	8,2	1,0

Table 12: Stack electrical efficiency under syngas

Time	U stack [V]	I stack [A]	Pelec [W]	**Eff HHV**	**Eff LHV**
690h	4,75	32	152,1	42,40	49,84
1130h	4,74	32	151,7	42,29	49,71
1440h	4,72	32	150,9	42,05	49,43

The three V-I curves and EIS spectra measured at the times denoted by the red stars in Figure 28 are compared in Figure 29 and Figure 30. The OCV for the start, middle and end are respectively 1.002 V, 1.005 V and 1.001V whereas under load the mean degradation is 8.2 mV/kh. Following Figure 30, both the ohmic and polarization resistances have increased. However, the interference of inductance and capacitance at high frequencies makes the ohmic resistance hard to evaluate. The DRT of Figure 31 and its peak details of Table 13 show that P1 and P2 have increased at the end of the baseline test, whereas the high frequency peaks decreased. As described in Caliandro [9], it looks as if the processes of charge transfer and diffusion of hydrogen are enhanced over time whereas the cathode process included in P1 seems to account for the increase of polarization resistance during the baseline operation. To check this assumption, two measurements at two different air flow rates were compared in Figure 32. The first peak P1 is definitely linked to cathodic processes. With a smaller flow rate, the resistance increases and the process is slowed. This seems to indicate that the air feed to the RUs was worsened over time, either due to obstruction or leakage.

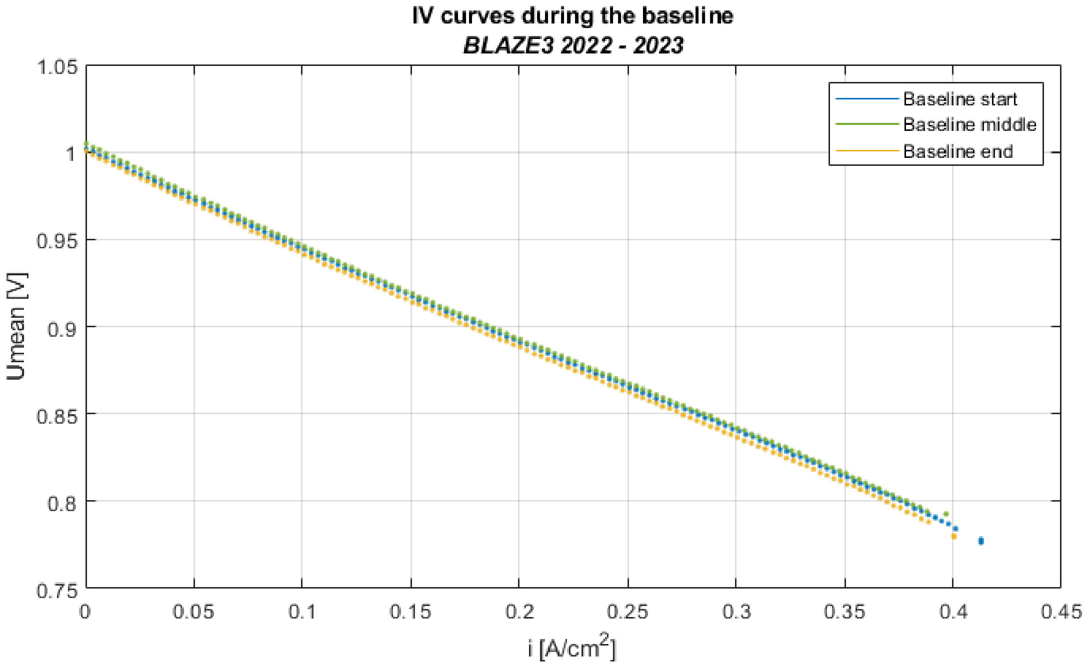

Figure 29: V-I curves measured at 1 A/min at the start, middle and end of the baseline test. The outlet air temperature at the beginning of the measurement was respectively 752°C, 751.2°C and 751°C

This project has received funding from the European Union's Horizon 2020 research and innovation programme under grant agreement No 815284

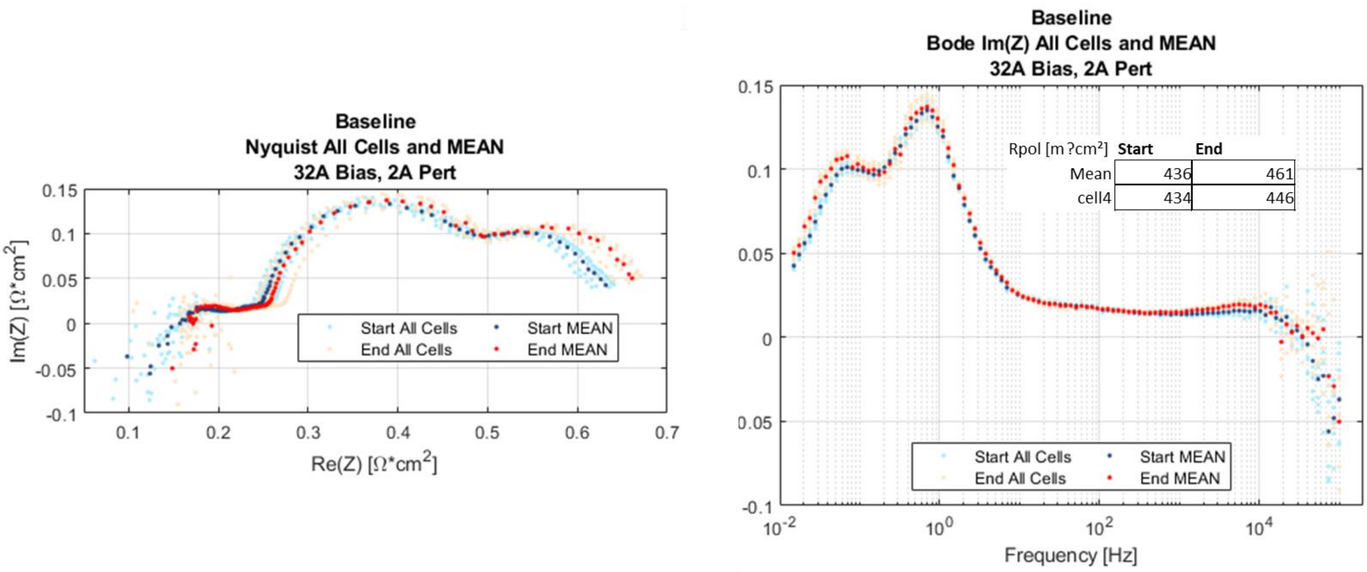

Rpol [m ?cm²]	Start	End
Mean	436	461
cell4	434	446

Figure 30: Nyquist (left) and Bode Im(Z) (right) under wood syngas#2 (69% H_2, 11% CO_2, 2% CH_4, 18% H_2O, 4.7 Nml/min/cm^2) at the start and end of the baseline test. The polarization resistance is estimated from the area under the Bode Plot (full spectrum) according to the Kramers-Krönig relation [5].

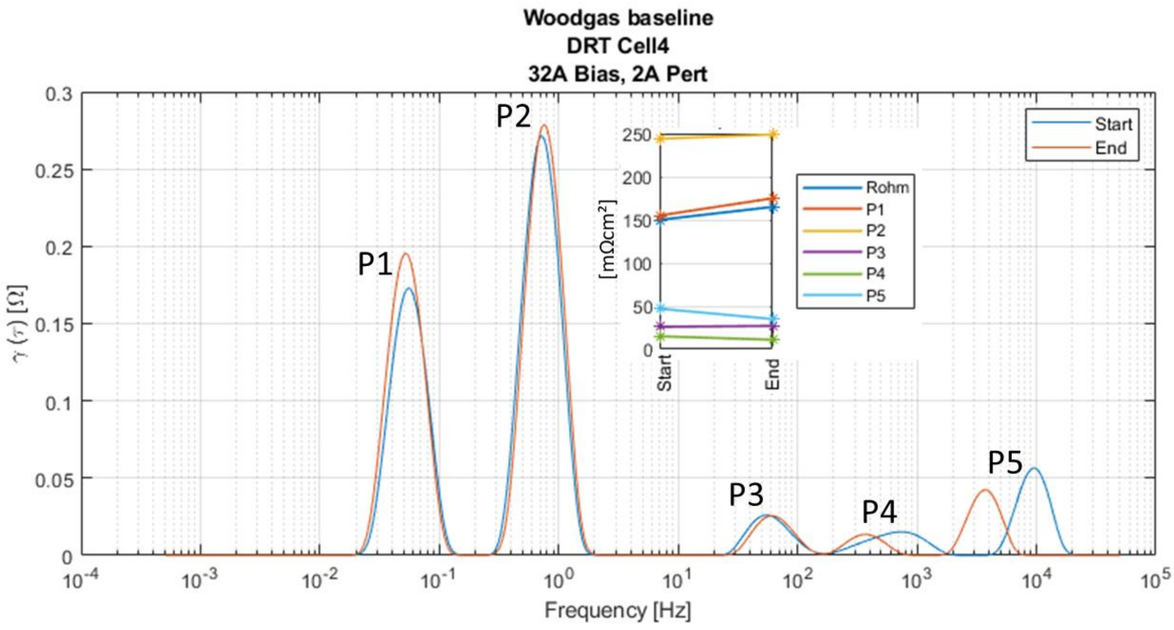

Figure 31: RU4 DRT under wood syngas#2 (69% H_2, 11% CO_2, 2% CH_4, 18% H_2O, 4.7 Nml/min/cm^2) at the start and end of the baseline test. Peak areas are displayed on the small chart (computed with peakfit).

Table 13: Detailed peak areas under wood syngas#2 (69% H_2, 11% CO_2, 2% CH_4, 18% H_2O, 4.7 Nml/min/cm^2) at the start and end of the baseline test. The polarization resistance is retrieved from the peaks sum. The ohmic resistance is estimated from the Nyquist plot.

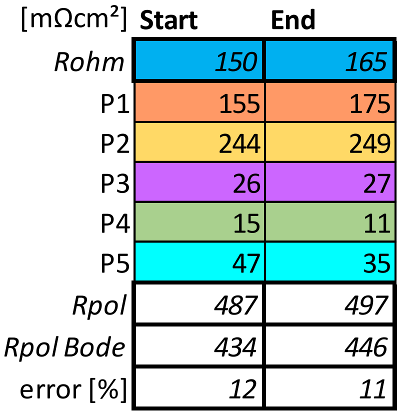

[mΩcm²]	**Start**	**End**
Rohm	*150*	*165*
P1	155	175
P2	244	249
P3	26	27
P4	15	11
P5	47	35
Rpol	*487*	*497*
Rpol Bode	*434*	*446*
error [%]	*12*	*11*

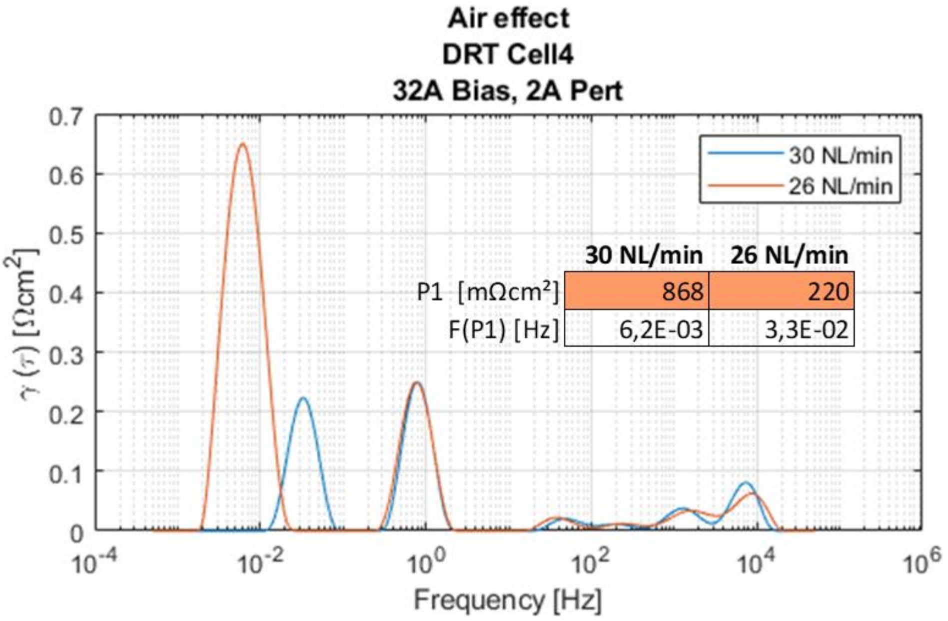

	30 NL/min	**26 NL/min**
P1 [mΩcm²]	868	220
F(P1) [Hz]	6,2E-03	3,3E-02

Figure 32: RU4 DRT at 30 NL/min and 26 NL/min of air.

4.4.3 Contamination

In total, the contamination phase lasted 1400 hours.

Introduction of the first level of DMS (0.5 ppm) started at 1500 h, the second level (1 ppm) was interrupted by the year-end break, stack#3 was left at OCV during that period. At 3000 h, 1 ppm of DMS was added again, the accounted measurements for that level are made after the break. To the contamination levels of DMS of 0.5, 1, 2, 3 and 4 ppm, three contamination levels of toluene were added (0, 100 and 400 ppm).

Figure 33 illustrates the cells voltages and the contaminant levels during the exposure to DMS and toluene. Figure 34 represents a zoom after the year-end break.

A delay of 40 h preceded the first sign of degradation. Indeed, all three stacks#1,#2,#3 experienced a delay of 25 h to 70 h after the first S-injection, before degradation was noticed. This phenomenon was also observed on the button cell tests from ENEA [11], where the voltage dropped only 48 h after 1 ppm of H_2S was injected. Also, Weber [12] reported a delay of 20 h for an anode supported button cell of 1 cm^2 contaminated with 0.1 ppm H_2S. Weber also stated that the amount of sulfur and the area of Ni surface will govern the onset of the degradation. As shown in stack#2 (Figure 21) and stack#3 later (Figure 39), the degradation starts when 70%-74% of the nickel area is covered. A larger Ni area and lower S-concentration will take longer to reach critical coverage.

In our short stack tests, the delay might also be affected by the test bench itself; though the impurity inlet pipe was protected with an inert alumina tube, sulfur could have adsorbed on the surface of the last few cm of unprotected metal before reaching the cells.

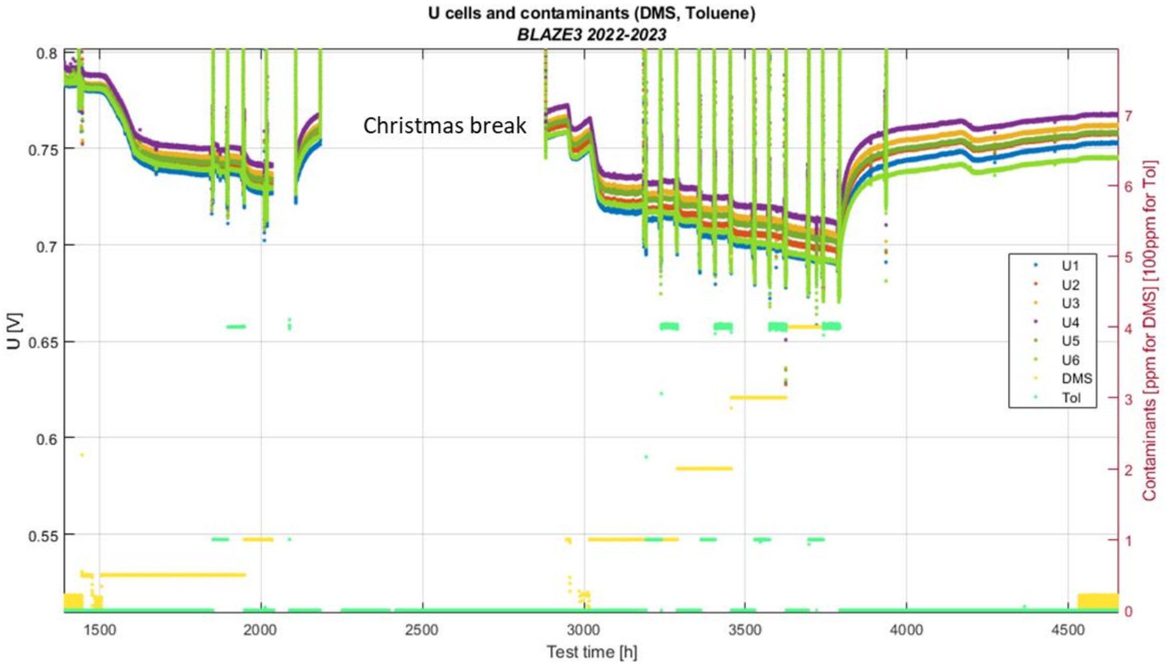

Figure 33: RU voltages during the contamination phases and recovery. Maximum 4 ppm of DMS (4ppm H_2S inside the cell) and 400 ppm of toluene were added.

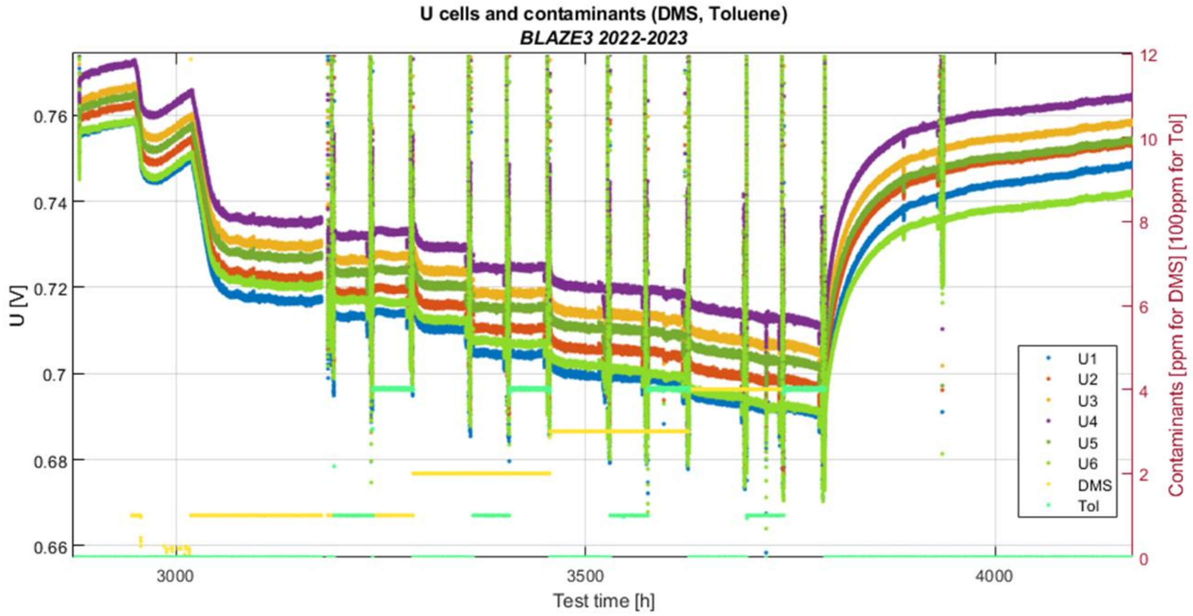

Figure 34: Zoom on the contamination phase after the year-end break (2022/2023). Maximum 4 ppm of DMS and 400 ppm of toluene were added. During the phase 1 ppm DMS + 0 ppm toluene and the phase 2 ppm DMS + 0 ppm toluene, the current was set to 31.7 A instead of 32 A due to a bias on the active load. Thus, the step change after these cases was not due to the addition of toluene but to this current correction.

The typical behaviour of sulfur exposure is observed here similarly to stack#2: a first voltage drop followed by a stable degradation rate. Those characteristics are presented in Table 14 (in mV) and in Table 15 (in %) for the different contaminant levels. The first voltage drop of stack#3 is 37.5 mV in 168 h. It is close to the observation on stack#2, that dropped 36.7mV in 65 h with 0.2 ppm of DMS. Unexpectedly, with the lower concentration of contaminant (0.2 ppm), performance dropped 2.6 times faster than with 0.5 ppm. Stack#2 started the exposure at a mean voltage of 0.770 V whereas stack#3 started at 0.780 V at nominal current, implying that a slightly healthier stack might take more time to reach a similar voltage drop and hence S-coverage. The stable degradation rate following the drop is also less prominent with the healthier stack#3 (14 mV/kh instead of 21 mV/kh for stack#2).

At 1 ppm DMS, the cumulative drop of stack#3 was 57.4 mV and 48.9 mV for stack#2. As the evolution of the voltages after 0.6 ppm DMS exposure on stack#2 are quite flat, it is hard to evaluate the time needed for the initial drop and to find a coherence in the evolution of the stable degradation rate along with the exposure. One reason is that the degradation is estimated over a rather short period (20 h to 100 h). It seems that the higher the contamination level, the higher the degradation rate. It also seems that a healthier stack shows a lower degradation rate, suggesting that the overpotential may play a role in the degradation mechanism.

The voltage drop attributed to the sulfur surface coverage (the total cumulative voltage drop without the added stable degradation phases) was 69.7 mV and the overall voltage loss during the whole contamination phase 83.1mV. Thus 84% of the overall performance loss was attributed to the sulfur alone.

Table 14: Mean potential loss during DMS and toluene exposition. A first drop is observed when the stack is exposed to DMS alone (2nd column) followed by a stable degradation rate (4th column). The degradation reported in the last two columns is under DMS and toluene combined. In green the voltages are increasing during the exposure phase. Degradation rates in mV/kh.

DMS conc [ppmv]	DeltaU before stabe degradation [mV]	Time for DeltaU [h]	Stable degradation rate [mV/kh]	Toluene degradation rate 100ppm [mV/kh]	Toluene degradation rate 400ppm [mV/kh]
0,5	37,5	168	13,8	15,2	4,1
1	19,9	54	2,2	21,4	16,0
2	6	15	11,4	23,3	4,1
3	4,2	16	20,8	12,5	27,9
4	2,1	10	30,4	35,9	44,7

Table 15: Potential loss during DMS and Toluene exposition. A first drop is observed when the stack is exposed to DMS alone (2nd column) followed by a stable degradation rate (4th column). The degradation reported in the last two columns is under DMS and toluene combined. In green the voltages are increasing during the exposure phase. Degradation rates expressed in %/kh

DMS conc [ppmv]	DeltaU before stabe degradation [%]	Time for DeltaU [h]	Stable degradation rate [%/kh]	Toluene degradation rate 100ppm [%/kh]	Toluene degradation rate 400ppm [%/kh]
0,5	4,8	168	1,9	2,0	0,6
1	2,7	54	0,3	3,0	2,2
2	0,8	15	1,6	3,3	0,6
3	0,6	16	2,9	1,8	3,9
4	0,3	10	4,3	5,1	6,4

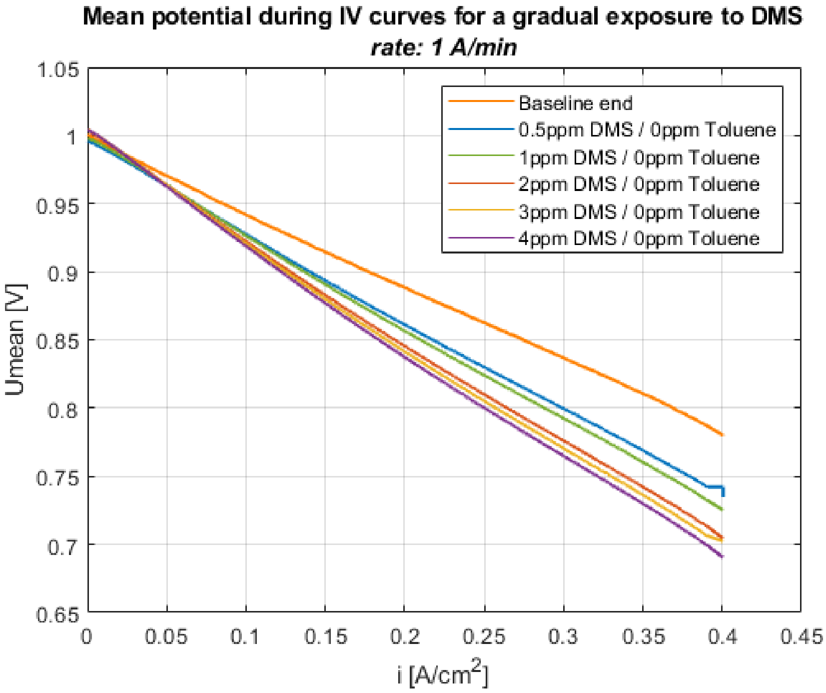

Figure 35: The V-I measured after the baseline test was recorded from stable OCV (current ramp: 1A/min). For the other V-I, the measurement started from stable nominal current (to 0A instantaneously, then V-I recorded) to minimize the time under sulfur contaminant without polarization.

An extended analysis of the effect of DMS is first presented in Figure 35, where V-I curves are measured at each level of DMS just before the addition of toluene. Clearly the slopes become steeper as the concentration of sulfur increases, whereas the OCV stays similar. However, the resistance associated with the slope is less impacted by the contaminant level once an initial catalyst coverage was made during a lower concentration exposure with DMS. E.g., the mean voltage at 0.4 A/cm^2 decreased by 6% after 0.5 ppm of exposure, but from 3 ppm to 4 ppm S-increase, the voltage drops by only a further 2%, similarly to the observation that the additional voltage drops became smaller when the sulfur concentration further rises.

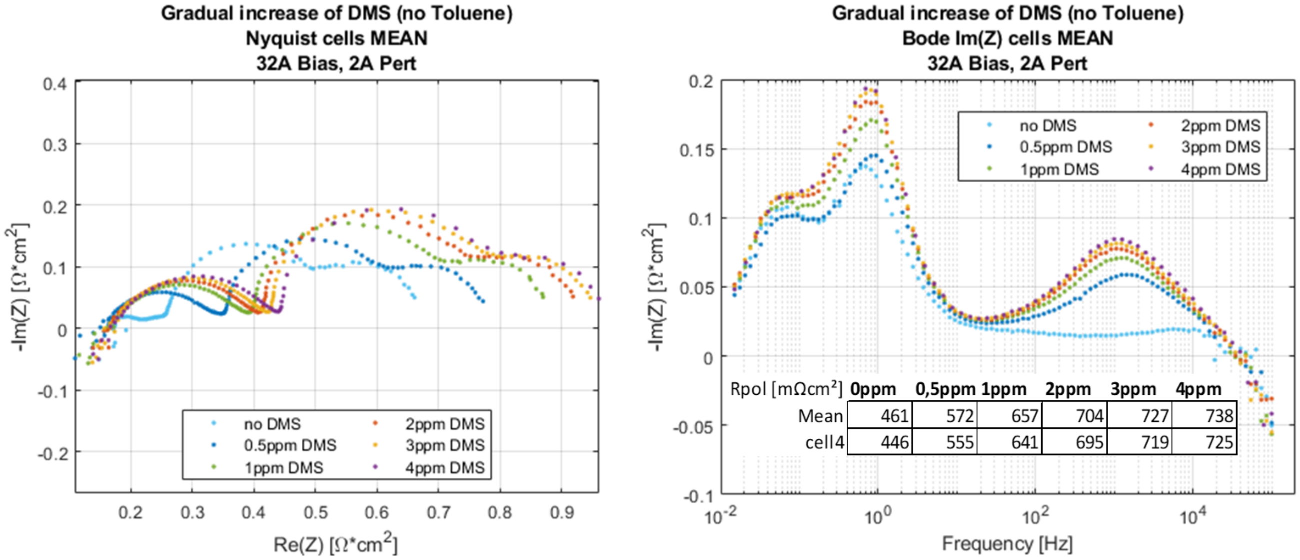

Rpol [mΩcm²]	0ppm	0,5ppm	1ppm	2ppm	3ppm	4ppm
Mean	461	572	657	704	727	738
cell4	446	555	641	695	719	725

Figure 36: Nyquist (left) and Bode Im(Z) (right) under wood syngas#2 (69% H_2, 11% CO_2, 2% CH_4, 18% H_2O, 4.7 Nml/min/cm^2, increasing levels of DMS added, cut at $10^4\ Hz$. The polarization resistance is estimated from the area under the Bode plot (full spectrum) according to the Kramers-Krönig relation [5].

After the V-I recording, impedance spectroscopy was performed. The EIS response from Figure 36 shows that the total resistance increases because of the increase in polarization resistance, whereas the ohmic resistance remains constant throughout the experiment. The sulfur coverage affects the polarization resistance in the frequency regions below 2 Hz and above 50 Hz. This is visible from the broadening of the Nyquist plot (the light blue curve, without DMS, has a shorter span), whereas the Bode plot informs on the frequency region (where the curves with contaminant lie above the light blue curve without contaminant). This is in line with stack#2 observations.

The DRT analysis of Figure 37 informs on the most impacted processes. Figure 38 represents the peak areas as a function of the DMS concentration. When comparing the measure before the contamination and at 0.5 ppm DMS, P4 and P5 are the most impacted peaks. P4 is generally attributed to charge transfer at the anode whereas P5 finds no consensus in literature and is expected to be affected by high frequency noise.[9]. In green, the P4 specific area is 6.8 times larger with 0.5 ppm DMS than without contaminant, showing that the active sites contaminated by sulfur have a higher resistance to the charge transfer. P2 shows a slight increase of 3%, P1 a decrease of 10%, back to the value at the beginning of the baseline test; hence this (cathode) process appears to have recovered.

Regarding the global evolution of the peaks with the increasing contamination, P2 and P4 show the most significant changes. Based on Table 16, in yellow, the gas conversion peak P2 increases for each new S-level by 3%, 23%, 10% and 5%, compared to the level before except for the last from 3 ppm to 4 ppm (0%). As the gas feed composition, the fuel utilization and the current density were constant throughout the test, the conversion resistance P2 can only be affected by the contaminant. This is consistent with the observations from Anke Hagen [13]. Using $H_2/H_2O/CO$ feed mixtures, she has shown that S-poisoning can affect the kinetics of the reverse water gas shift reaction (RWGS), thereby modifying the gas composition and resulting in a significant increase of the conversion impedance as measured by EIS. As the catalyst is partially deactivated, the internal reforming reaction should also be hindered decreasing the amount of hydrogen. However, as the share of methane is small, the combined effect of the slower RWGS and the slower methane reforming is still an increase of hydrogen. In Figure 43, the fuel outlet gas composition is analyzed and even though the increase of hydrogen throughout the contamination is not visible, the increase of methane is clear.

In green, P4 increases for each successive S-level by 582%, 79%, 0%, 11% and 5%, compared to the level before.

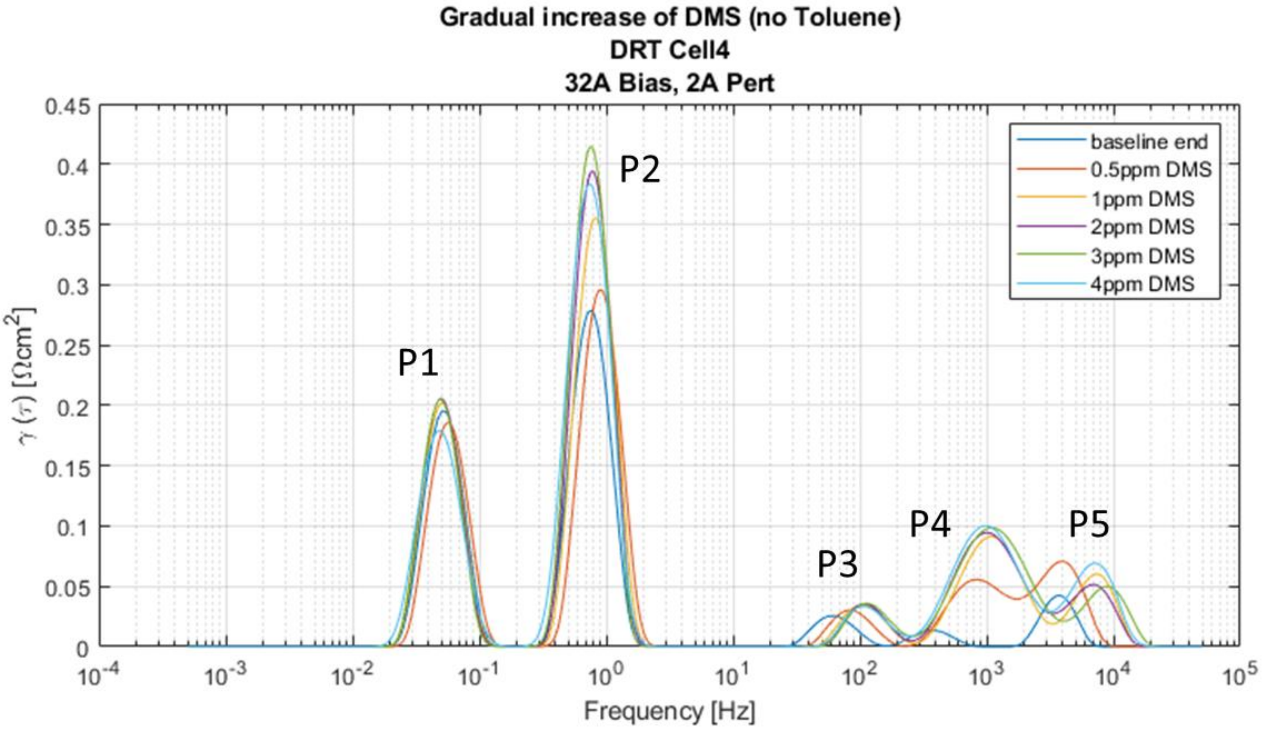

Figure 37: Cell#4 DRT under wood syngas#2 (69% H_2, 11% CO_2, 2% CH_4, 18% H_2O, 4.7 Nml/min/cm^2) under increasing concentration of DMS, just before toluene was added.

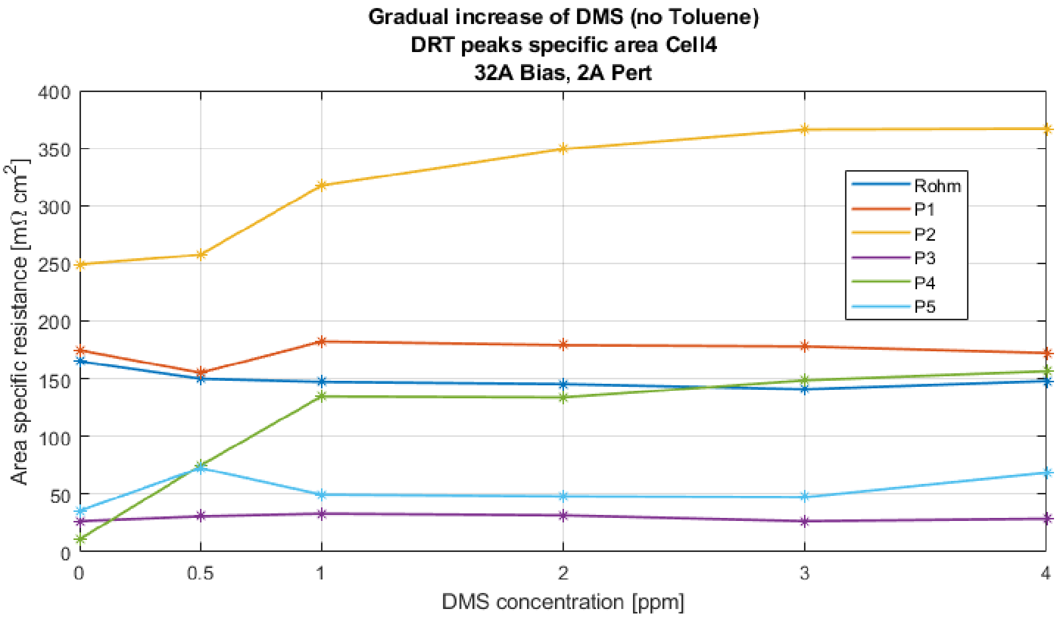

Figure 38: Area specific ressitance of the ohmic resistance and the 5 peaks P1-P5 of the polarization resistance, under increasing concentration of DMS, just before toluene was added.

Table 16: Detailed peaks area under wood syngas#2 (69% H_2, 11% CO_2, 2% CH_4, 18% H_2O, 4.7 Nml/min/cm^2) with increasing concentration of DMS, just before toluene was added. The polarization resistance is retrieved from the peaks sum and from the area under the Bode plot. The ohmic resistance is estimated from the Nyquist plot.

			0ppm Toluene			
[mΩcm²]	**0ppm**	**0,5ppm**	**1ppm**	**2ppm**	**3ppm**	**4ppm**
Rohm	*165,0*	*150,0*	*147,3*	*145,4*	*140,9*	*148,0*
P1	174,7	155,1	182,1	179,0	177,9	172,3
P2	249,1	257,5	317,4	349,1	366,0	366,7
P3	26,6	30,7	33,0	31,6	26,6	28,7
P4	10,7	74,6	134,5	133,7	148,6	156,4
P5	35,4	72,5	49,6	48,1	47,3	68,4
Rpol	497	590	716	742	766	792
Rpol Bode	*446*	*555*	*641*	*695*	*719*	*725*
error [%]	*11*	*6*	*12*	*7*	*7*	*9*

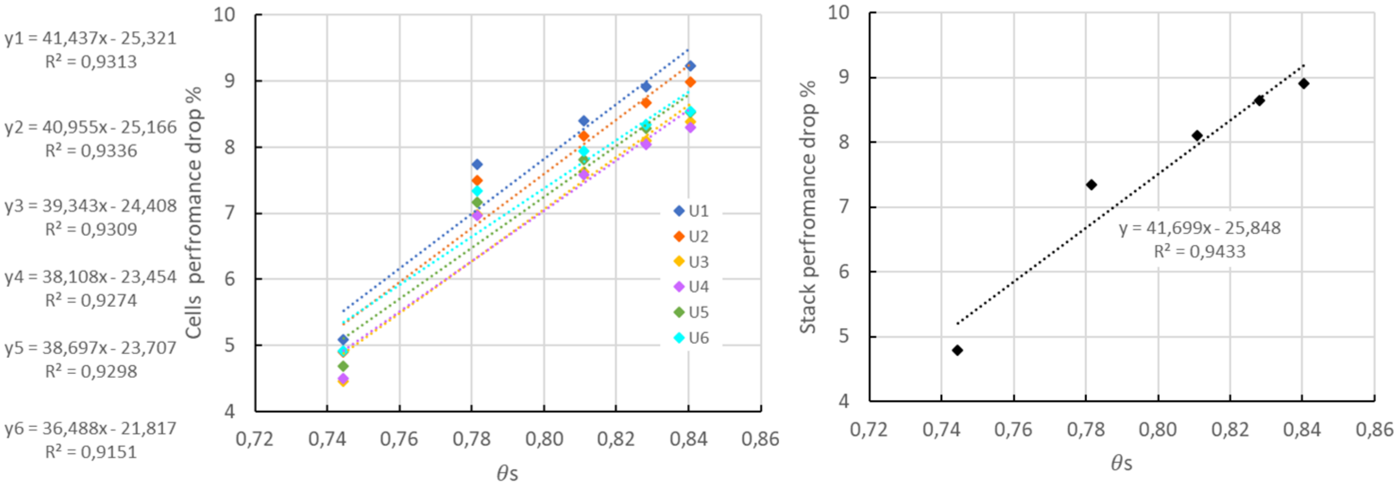

Figure 39: Cell performance drop as a function of the sulfur surface coverage θ_s. Left: cell#1 to cell#6 linear regression and plot. Right: stack linear plot and regression.

As already mentioned, the loss of performance and thus the increase of resistance is correlated to the sulfur coverage of the nickel catalyst. John Hansen suggested to describe the covered fraction of the catalyst surface in terms of a Temkin adsorption isotherm [10]:

$$\theta_s = 1.45 - 9.53 \cdot 10^{-5} T + 4.17 \cdot 10^{-5} T ln(H_2S/H_2)$$

where θ_s is the surface coverage fraction and T (K) the temperature at the triple phase boundary. Here the air outlet temperature was used as the reference temperature. The surface coverage ranges from 0.74 to 0.84 for DMS concentrations from 0.5 ppm to 4 ppm. The linear relationship between the cumulative performance loss and the surface coverage is plotted in Figure 39 where the voltage loss considered is the voltage drop before the stable degradation phase, as this phase is believed to arise from other processes than the coverage process itself. The linear fit seems to reflect the process, as R^2 is higher than 0.9, confirming Hansen's assumption that the voltage drop is proportional to the surface coverage.

As Hansen suggests, the minimum coverage needed for a performance loss can be extracted:

$$y_i = a\theta_s - b = a(\theta_s - \theta_{min}) \quad \rightarrow \quad \theta_{min} = \frac{b}{a}$$

The minimum coverage needed ranges from θ_{min} = 0.6 for the least efficient cell to θ_{min} = 0.64 for the better ones. Despite such a high value, the H_2S concentration leading to such coverages is very low, respectively 19 ppb and 33 ppb.

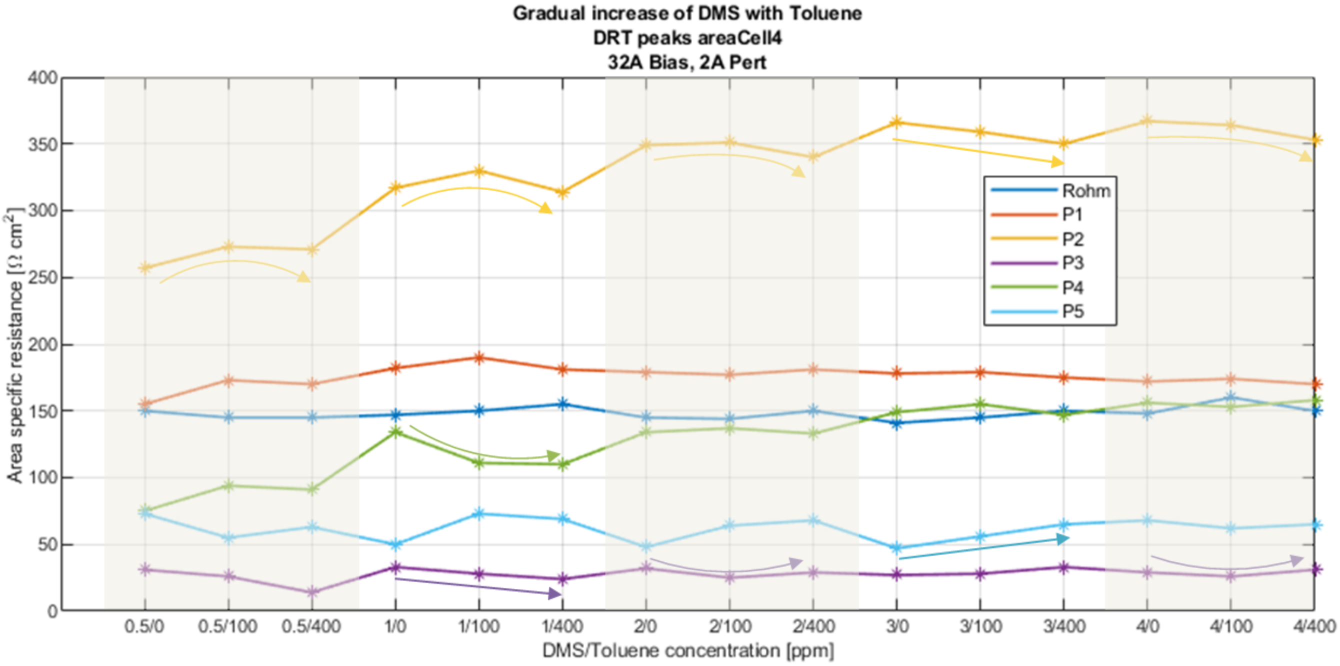

Figure 40: Area specific resistance of the ohmic resistance and the 5 peaks P1-P5 of the polarization resistance under increasing concentration of DMS and toluene.

Table 17: Detailed peaks area under wood syngas#2 (69% H_2, 11% CO_2, 2% CH_4, 18% H_2O, 4.7 Nml/min/cm^2) with increasing concentration of DMS, with addition of toluene. The polarization resistance is retrieved from the peaks sum and from the area under the Bode plot. The ohmic resistance is estimated from the Nyquist plot.

	0ppm	**0,5ppm DMS**			**1ppm**			**2ppm**			**3ppm**			**4ppm**		
[mΩcm²]	**0ppm Tol**	**0ppm**	**100ppm**	**400ppm**	**0ppm**	**100ppm**	**400ppm**	**0ppm**	**100ppm**	**400ppm**	**0ppm**	**100ppm**	**400ppm**	**0ppm**	**100ppm**	**400ppm**
Rohm	*165,0*	*150,0*	*145,0*	*145,0*	*147,3*	*150,0*	*155,0*	*145,4*	*144,3*	*150,0*	*140,9*	*145,0*	*150,0*	*148,0*	*160,0*	*150,0*
P1	174,7	155,1	172,7	169,7	182,1	190,0	180,7	179,0	177,1	180,9	177,9	178,9	174,6	172,3	174,2	169,6
P2	249,1	257,5	273,0	271,2	317,4	330,3	313,7	349,1	350,8	339,9	366,0	358,9	350,2	366,7	363,5	353,3
P3	26,6	30,7	26,0	14,1	33,0	28,2	23,9	31,6	25,3	28,5	26,6	27,8	33,2	28,7	26,2	31,3
P4	10,7	74,6	94,3	91,5	134,5	110,8	110,4	133,7	136,7	132,8	148,6	155,2	147,1	156,4	152,7	158,2
P5	35,4	72,5	54,6	62,6	49,6	72,7	68,7	48,1	63,6	67,8	47,3	56,2	64,5	68,4	62,1	65,0
Rpol	497	590	621	609	716	732	697	742	754	750	766	777	770	792	779	777
Rpol Bode	*446*	*555*	*567*	*568*	*641*	*662*	*636*	*695*	*698*	*683*	*719*	*712*	*704*	*725*	*720*	*714*
error [%]	*11*	*6*	*9*	*7*	*12*	*11*	*10*	*7*	*8*	*10*	*6*	*9*	*9*	*9*	*8*	*9*

The effect of toluene addition was investigated through DRT analysis. On one hand, Figure 40 shows the area of the 5 peaks as well as the ohmic resistance, for all levels of exposure. On the other hand, the peak frequencies during the exposure are presented in Figure 41. The conversion peak P2 is again the most impacted one in terms of area specific resistance. It looks like the toluene moderates the impact of H_2S as the peak area is decreased at 400 ppm toluene for all DMS levels and already at 100 ppm toluene for 2 ppm to 4 ppm DMS. However, to confirm this ‘positive’ effect of toluene, it would be necessary to understand better the evolution of P2 with a constant contamination of DMS over several days with regular EIS measurements. A similar behaviour was observed for P4, as well as P3 and P1 for 0.5 ppm and 1 ppm of DMS. On the contrary, P5 seems to increase with the addition of toluene starting from 1 ppm of DMS. However, when the toluene is again removed, the resistance of that peak again decreases until 4 ppm of DMS, where the resistance stays stable.

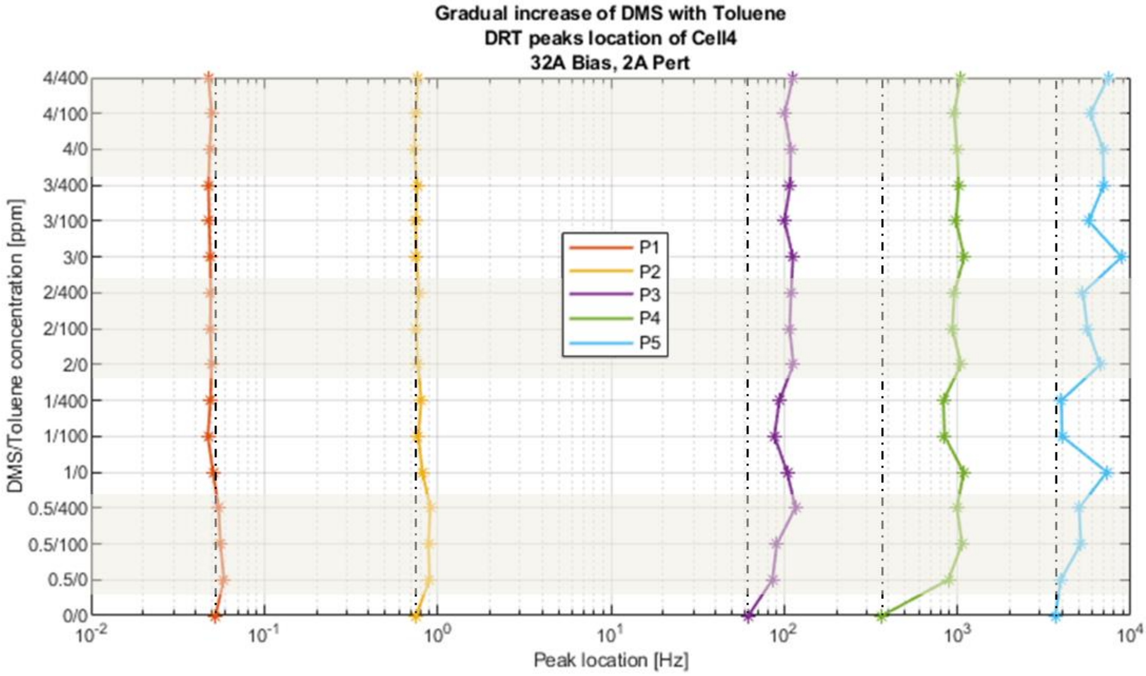

Figure 41: Peak frequencies locations under increasing concentration of DMS and toluene.

P3 and P4 (anode charge transfer process) show a significant drift towards higher frequencies after the first sulfur surface coverage.

4.4.4 Gas analysis

According to Figure 42, the inlet gas composition of the main gas components is constant throughout the test. It matches the expectation as the measurement is performed before the stack inlet, in the furnace at 750°C. (The measurement at 3 ppm DMS/ 100 ppm toluene is likely an outlier.) On the one hand, the thermal equilibrium simulated with the software HSC (Table 18) shows that CH_4 will largely be reformed to CO and H_2. If the total hydrogen content decreased, the reverse water gas shift would be active and transform H_2 and CO_2 partly into CO and H_2O. On the other hand, the gas analysis shows that the measured gases are similar to the set composition. Thus, the RWGS is inactive upstream the stack inlet (homogeneous reaction), as expected.

Focusing on the outlet gas composition, the methane share increases slowly but significantly throughout the contamination phase as seen in Figure 43. It seems that the CH_4 amount increases at each new level of DMS and reaches a plateau until the DMS level is further increased. This observation supports the suggestion of a maximum sulphur coverage of the active area for a given H_2S concentration. The covered nickel catalyst will lead to a slower rate of reaction of the gas mixture to reach thermodynamic equilibrium.

A slower methane reforming reaction will preserve CH_4 which will also cause a decrease of H_2 and CO concentration. However, a CO decrease is noticeable but only from 2 ppm of DMS. A temporary faster rate of reaction of the RWGS could contribute to this constant value of CO, which would in addition decrease the hydrogen content until 2 ppm of sulfur, and increase after 2 ppm. CO_2would also increase from 2 ppm of sulfur due to the slower rates of both the (dry) reforming and the reverse water gas shift reactions. Those trends aren't clearly visible on the output composition of Figure 43 but neither conflict with this assumption as both H_2 and CO_2wobbles around a constant value. A point that is more delicate is the fact that the conversion losses increase right from the beginning of the injection of DMS whereas the latter explanation would increase the steam content and thus decrease P2 area.

From the toluene contaminations, no significant impact is visible on the gas outlet measurement. When the contamination ceased, the methane concentration quickly returned to the initial level. Likewise, CO and H_2 re-increase, in line with the steam methane reforming being active again.

Table 18: Inlet gas composition (set point, thermodynamic equilibrium (HSC), Micro-GC measurement (3% N_2 and O_2 removed and % adapted)

Composition [%]:	**H2**	**CH4**	**CO**	**CO2**
Inlet set point [% dry]	84,1	2,4	0	13,4
Inlet HSC software simulation [% dry]	83,8	0,3	11,0	4,9
Inlet measurement microGC	81,7	2,8	0,4	15,1

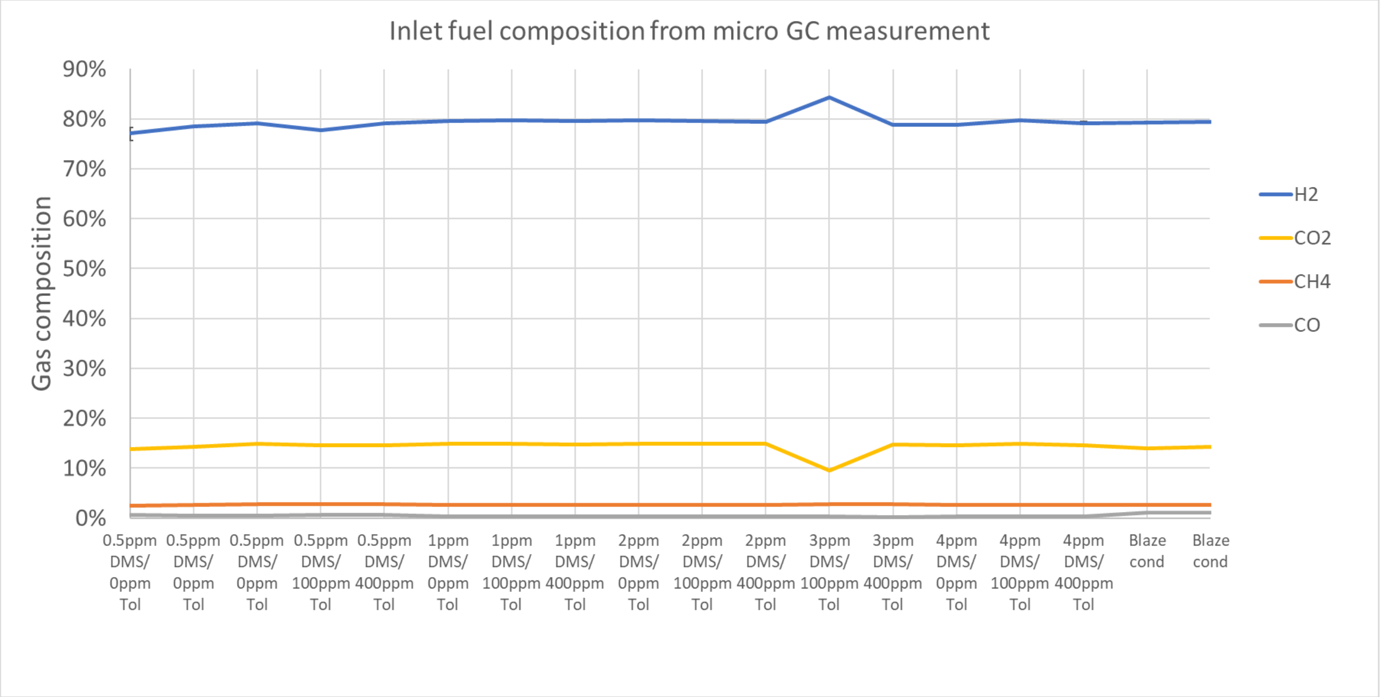

Figure 42: Dry inlet anode gas composition during the contamination phase. Mean value of 3 measurements from the Micro-GC. The first level of contamination lasted 22 days without toluene, then each condition lasted 2 days. After the contamination, a measurement is performed after 4 days and another after 2 days

more. The measurement at 3 ppm DMS/ 0 ppm Tol(uene) had outlier values and is not shown here. No values are available before the contamination. Error bars are plotted based on the max and min value from the 3 measurements. The width of the lines is chosen for clarity but hides the small error bars.

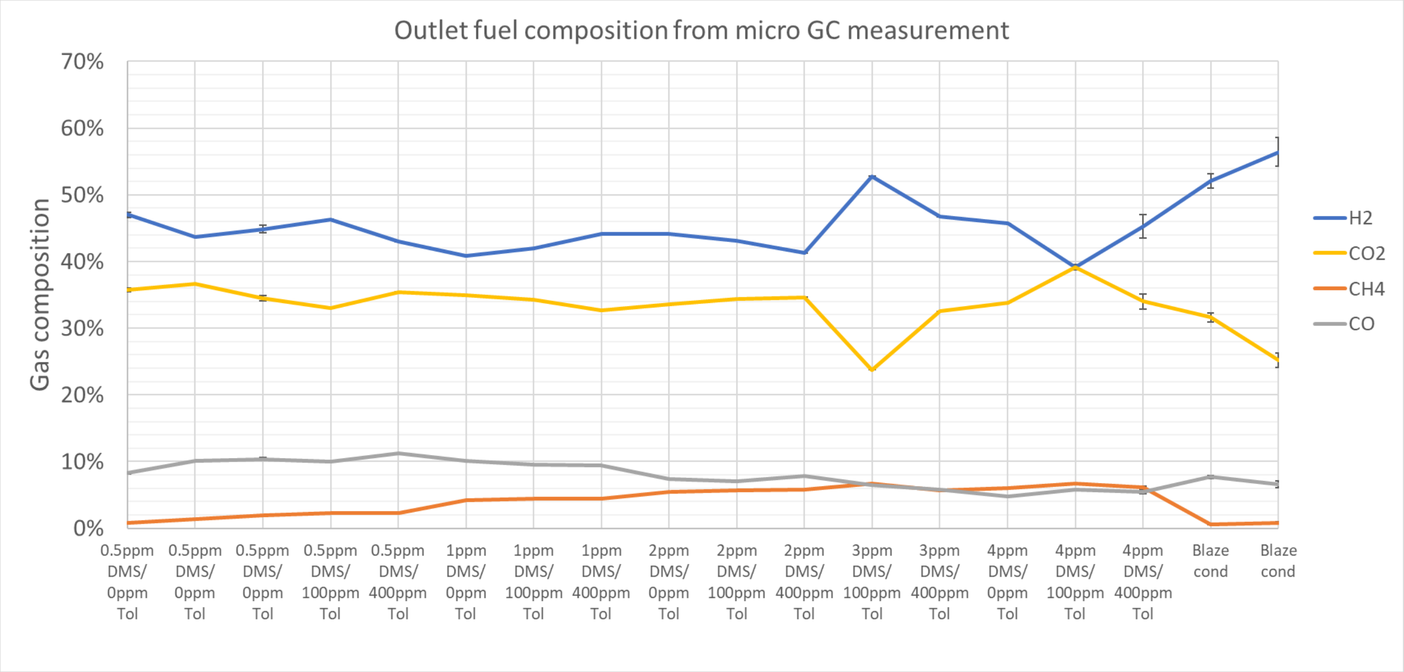

Figure 43: Dry outlet anode gas composition during the contamination phase. Measurement from the Micro-GC. The first level of contamination lasted 22 days without toluene, then each condition lasted 2 days. After the contamination, a measurement is perfromed after 4 days and another after 2 days more. The measurement at 3 ppm DMS/ 0 ppm Tol(uene) was an outlier and is not shown here. No values are available before the contamination. Error bars of the 1st, 3rd and the 4 last points are plotted based on the max and min value from the 3 measurements.

4.4.5 Recovery

When a RU voltage dropped below 0.7V, the contaminants injection was stopped and the stack was kept polarised at 32 A under wood syngas condition (SG2). After 2400 h contaminant free operation (14,4 weeks), the stack recovered 76% of its initial performance, just before a new contamination sequence. The recovery is logarithmical: the time needed to recover 38% was only 33 h, and the one to recover 60% was 250 h. Compared to the total voltage drop caused by the sulfur coverage (69.7 mV), 91% (63.2 mV) was recovered. In other words, it seems plausible that the voltage loss due to sulfur contamination could eventually be almost fully recovered, after several 1000h; the unrecovered part (here 24% after 2400h) would then be mostly ascribed to processes that degraded for other reasons than contaminant exposure.

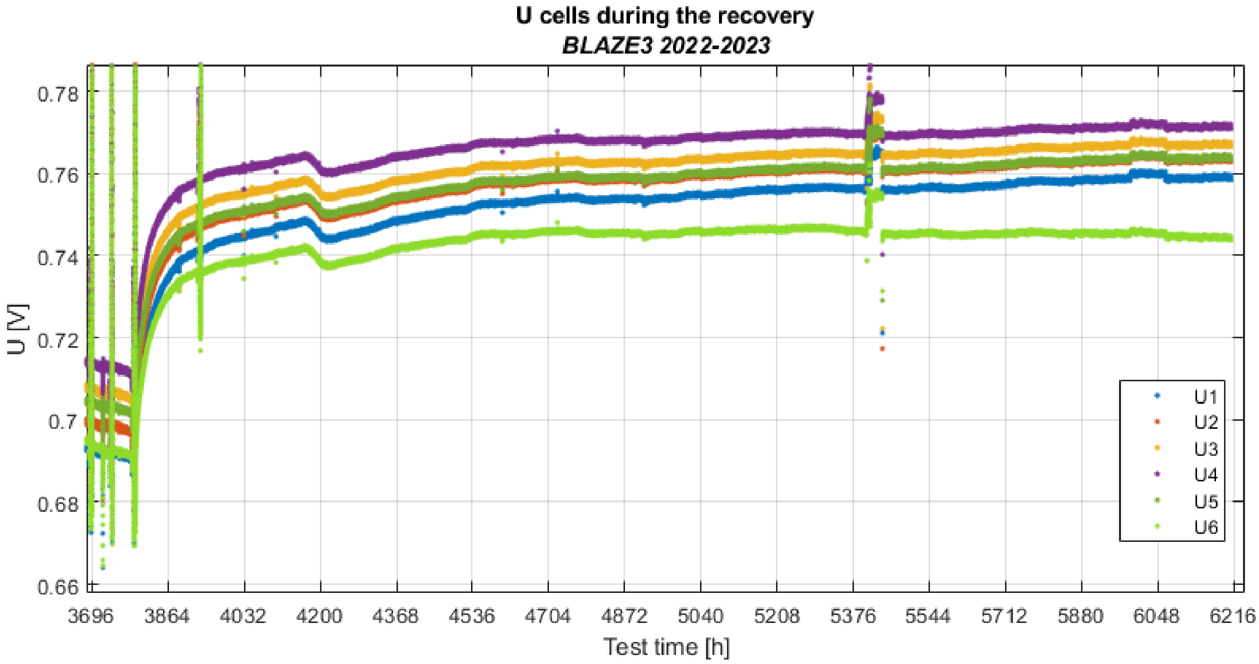

Figure 44: RU potentials during the recovery phase. 1 week (168h) separates each vertical grid line. The step at 4200 h could not be attributed to any measured stack condition parameter such as pressure or temperature.

4.4.6 HCl contamination

Before the final addition of HCl, stack#3 was still slowly recovering, as shown above. Figure 45 shows the RU potentials starting from the first contaminant level of 5 ppm HCl (in N_2). As the injection started, the performance decreased steeply during the first 10 h at -220 mV/kh and then reached a stable degradation rate of -60 mV/kh that stayed similar during the following contamination levels of HCl up to 50 ppm. Unfortunately, data acquisition stopped during the transition of 20 ppm to 50 ppm of HCl; the potentials look as if a small step occurred during this transition. According to the steady degradation rate of -60 mV/kh, at the time the acquisition restarted, the potentials would be 1 mV higher. It is suspected to come from the dilution of reducing fuel, with the addition of nitrogen, as 226 Nml/min N_2 was added at 50 ppm HCl, resulting in a 1 mbar increase at the fuel inlet. When the exposure to HCl was interrupted, the potentials jumped instantaneously by 1 mV, however, the performance continued to degrade, though at a milder rate of -43 mV/kh.

EIS measurements were performed at the end of each contaminant level. DRT analysis is presented in Figure 46 and a zoom on the high frequency peaks can be found in Figure 47. The changes observed at low frequencies are rather small (P1, P2 and P3); nonetheless, P1 increased by 10 $m\Omega cm^2$ after the addition of HCl. Surprisingly, a 6th peak appeared, already at 0 ppm of HCl, which alters the numbering of the peaks compared to the previous sections. The specific resistances of P4 to P6 were not evaluated as peakfit.m was not able to fit properly the DRT output, even when reducing the frequency domain. This is true especially for 10 ppm HCl where P4 is almost vanished between P3 and P5. A manual integration was not possible as the peaks are overlapping each other. The areas of P1, P2 and P3 are presented in Table 19 as well as the polarization resistance from the DRT plot, the polarization from the Bode plot (not shown) and the error between the Bode plot and the DRT fit.

First, the error was significantly higher (median error 16%) than those of the sulfur/toluene test campaign (median error 9%). The Z-HIT, the DRT fit from DRTtools and the peak fits from peakfit.m of a measurement at 9% error and one at 16% error can be found in Appendix 7.1.1.7. The error arises mainly from the high frequencies and the 6th peak could be an artefact.

Second, P1 has a specific area 30% higher than during the sulfur test campaign. The air flow rate was set to 30 NL/min instead of 32 NL/min and, as seen previously, a lower airflow affects P1.

The performance loss is attributed to a small ohmic resistance increase of around 10 $m\Omega cm^2$ and to a polarisation resistance increase of around 20 $m\Omega cm^2$ both at low and at high frequencies. HCl seems to have small impacts, but on a wide range of processes including fuel diffusion and charge transfer. Apparently, it is not covering the catalyst, as the conversion peak P2 stays unchanged throughout the test.

Gas analyses were carefully carried out, but no trends could be recognized.

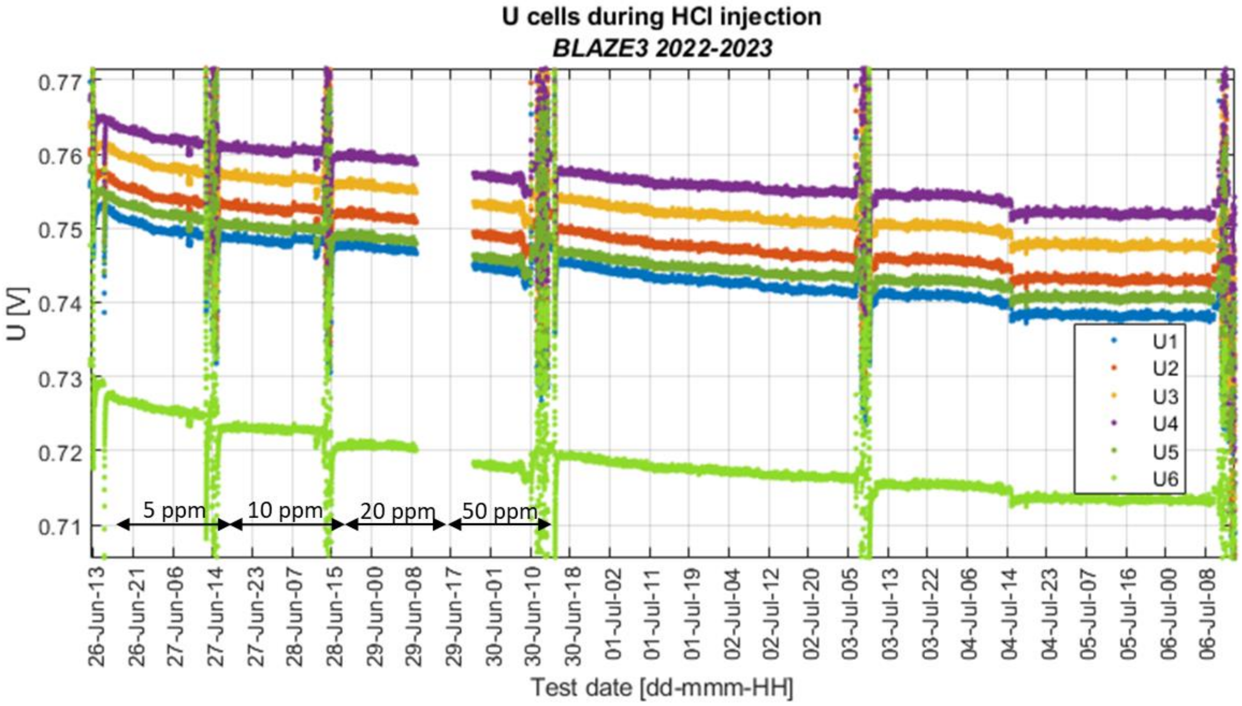

Figure 45: RU potentials during exposure to HCl, plus 6 days without impurity. Data acquisition stopped between 20 ppm and 50 ppm of HCl.

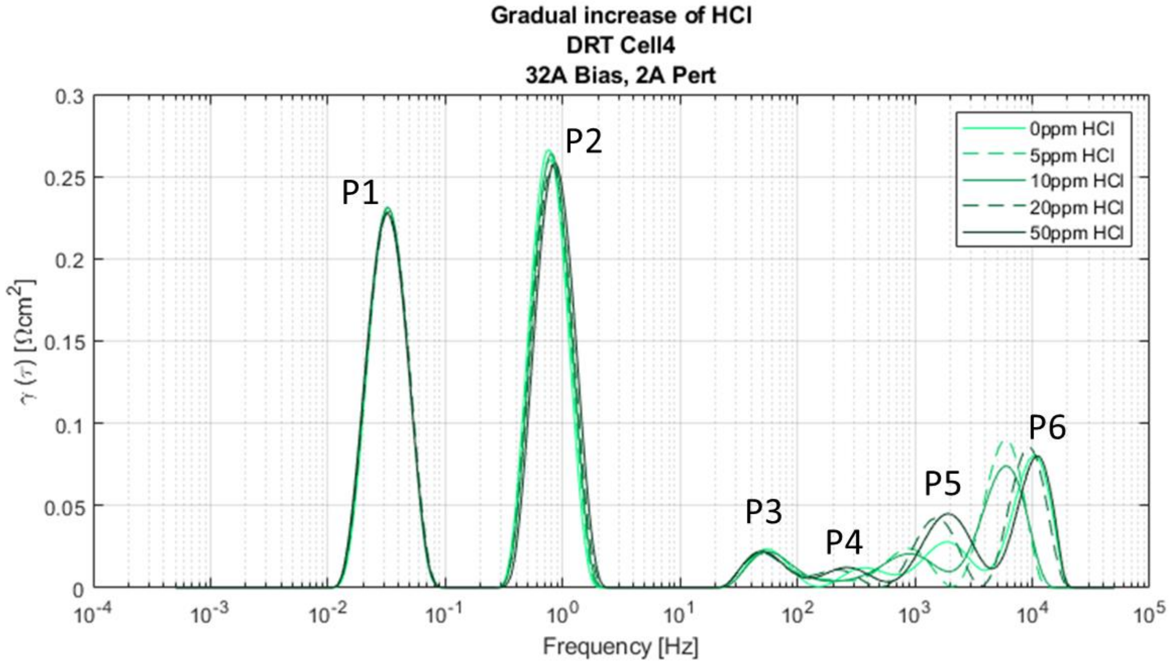

Figure 46: RU4 DRT under wood syngas#2 (69% H_2, 11% CO_2, 2% CH_4, 18% H_2O, 4.7 Nml/min/cm^2) during a gradual increase of HCl.

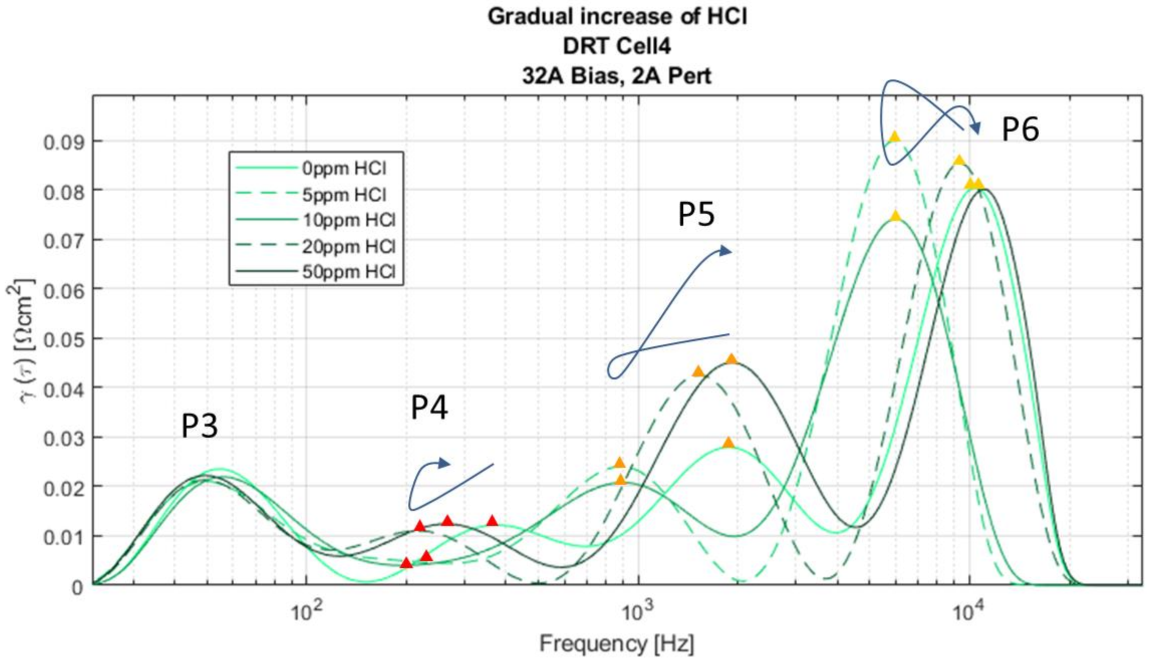

Figure 47: RU4 DRT zoom on frequencies from 10 Hz to $3 \cdot 10^4$ Hz where P3 to P6 appear.

Table 19: Detailed peak areas under wood syngas#2 (69% H_2, 11% CO_2, 2% CH_4, 18% H_2O, 4.7 Nml/min/cm^2) with increasing concentration of HCl. The polarization resistance is retrieved from the peaks sum (and does not reflect well the high frequencies resistance as peakfit was not fitting well) and from the area under the Bode plot. The ohmic resistance is estimated from the Nyquist plot.

[mΩcm²]	**0ppm**	**5ppm**	**10ppm**	**20ppm**	**50ppm**
Rohm	*165*	*175*	*180*	*175*	*175*
P1	214	224	225	221	221
P2	242	243	246	241	245
P3	20	20	22	22	19
Rpol	592	593	593	608	617
Rpol Bode	512	516	504	526	529
error [%]	16	15	18	15	17

5 CONCLUSIONS

Three short stacks from SOLIDpower/SolydEra were tested under conditions mimicking their operation with syngas produced by the steam gasification of woody biomass.

The first stack#1 was operated **9000 h** in steady conditions at 0.4A/cm^2 and 80%FU, setting the **baseline degradation** rate without the injection of impurities. Most RU showed an ‘expected’ degradation rate (-3.4 mV/kh, -0.4%/kh) except the last RU (cell6) that started degrading strongly after 3000 h (-26 mV/kh, -3.3%/kh). EIS measurements showed that the degradation was mainly due to an increase in the **ohmic** losses.

The second stack#2 was also operated **9000 h** in total, including **2000 h with impurities**. The stack had undergone 6 unplanned emergency stops and had therefore already degraded before impurities were injected. The contaminants were an organic sulfur compound (DMS, 0.2-1.6 ppm) and a light tar (toluene, 20-180 ppm). **Sulfur had a strong impact** on the performance of the stack even at the lowest level (**0.2 ppm**). It was shown that the loss of performance was linearly proportional to the Ni-surface sulfur coverage, assuming a Temkin-like isotherm. This was confirmed by EIS, which showed that S-poisoning increased the charge transfer resistance (P4) at the electrolyte/anode interface and hindered the RWGS reaction (P2), both catalysed by Ni. The impediment of the internal methane refroming was also witnessed through gas chromatography measurements. The addition of **toluene up to 180 ppm did not have any impact** on the stack performance.

These observations were confirmed during the tests with the third stack#3, which lasted **4500 h** altogether, with **1000 h** of impurity injection up to 4 ppm DMS and 400 ppm Toluene. In addition to the previous observations, it was shown that co-feeding of toluene with DMS could have a somewhat ‘beneficial’ action on mitigating the poisoning of Ni by sulfur. Another observation worth mentioning is that after stopping the injection of impurity, the **stack recovered 50% of its performance within 33h and 80% within 250h.** And potentially full recovery after several thousands of hours.

Using the Temkin-like isotherm suggestion, a maximum sulfur coverage that would not generate any additional degradation was estimated to 64%, corresponding to an allowable sulfur level in the fuel of only 30 ppb, showing how strong nickel interacts with sulfur.
On average over stack#2 and stack#3, the total voltage loss for 0.2 ppm and 1 ppm of sulfur is respectively 40 mV and 55 mV.

6 REFERENCES

[1] Poling, Bruce E., John M. Prausnitz, and John P. O'connell. *Properties of gases and liquids*. McGraw-Hill Education, 2001.

[2] Ehm, W, Gohr, H., Kaus, R., Roseler, B., & Schiller, C. A. (2000). The evaluation of electrochemical impedance spectra using a modified logarithmic Hilbert transform. *ACH MODELS IN CHEMISTRY*, *137*(2/3), 145-158.

[3] T.H. Wan, M. Saccoccio, C. Chen, F. Ciucci, Influence of the Discretization Methods on the Distribution of Relaxation Times Deconvolution: Implementing Radial Basis Functions with DRTtools, Electrochimica Acta, 184 (2015) 483-499.

[4] Tom O'Haver. Interactive Peak Fitter. URL

[5] Macdonald, D. D., & Urquidi-Macdonald, M. (1985). Application of Kramers-Kronig Transforms in the Analysis of Electrochemical Systems: I. Polarization Resistance. *Journal of the Electrochemical Society*, *132*(10), 2316.

[6] Hossein Madi, Stefan Diethelm, Christian Ludwig, Jan Van herle, Organic-sulfur poisoning of solid oxide fuel cell operated on bio-syngas, Int. J. of hydrogen energy 41 (2016) 12231-12241

[7] John Bøgild Hansen, Correlating Sulfur Poisoning of SOFC Nickel Anodes by a Temkin Isotherm, Electrochemical and Solid-State Letters, 11 (10) B178-B180 (2008)

[8] Caliandro, Priscilla. *Identification of Solid Oxide Cell Elementary Processes by Electrochemical Impedance Spectroscopy*. No. THESIS. EPFL, 2018.

[9] Anke Hagen, Sulfur Poisoning of the Water Gas Shift Reaction on Anode Supported Solid Oxide Fuel Cells, Journal of The Electrochemical Society, 160 (2) F111-F118 (2013)

[10] Hansen, John Bøgild. "Correlating sulfur poisoning of SOFC nickel anodes by a Temkin isotherm." *Electrochemical and Solid-State Letters* 11.10 (2008): B178.

[11] Davide Pumiglia, Massimiliano Della Pietra, Andrea Monforti Ferrario, Stephen J. McPhail (ENEA). BLAZE D3.3 "Report summarising the button cell tests"

[12] Weber, André, et al. "Sulfur poisoning of anode-supported SOFCs under reformate operation" *Fuel Cells* 13.4 (2013): 487-493.

[13] Anke Hagen, Sulfur Poisoning of the Water Gas Shift Reaction on Anode Supported Solid Oxide Fuel Cells, Journal of The Electrochemical Society, 160 (2) F111-F118 (2013)

7 APPENDIX

7.1.1.1 Cells voltages during the exposure to 0.5 ppm of DMS

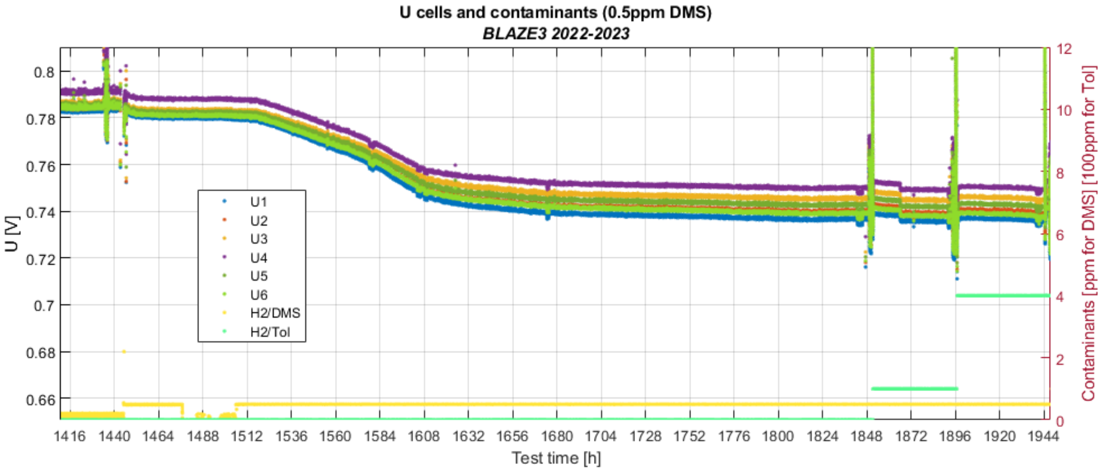

Figure 48: Contamination phase = 0.5 ppm DMS. Cell potentials on the left axis. DMS and toluene concentration on the right axis (read 100 ppm and 400 ppm for the toluene concentration).

The current throughout this contamination phase was 32 A. The step at 1865 hours is the late adjustment of the hydrogen flow rate.

7.1.1.2 Cell voltages during the exposure to 1 ppm of DMS

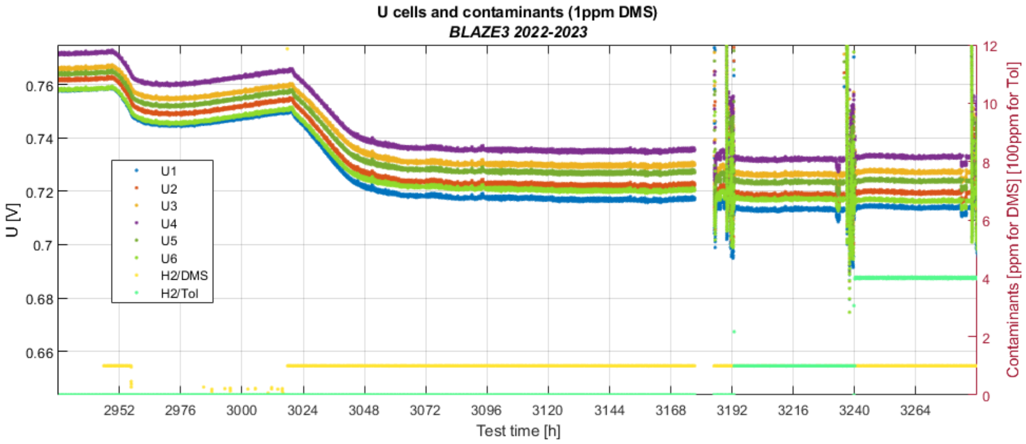

Figure 49: Contamination phase =1 ppm DMS. Cell potentials on the left axis. DMS and toluene concentration on the right axis (read 100 ppm and 400 ppm for the toluene concentration).

The current throughout this phase was 31.7A until 3192 h (the active load has an offset of 0.3A). After adding toluene, I was correctly set to 32A.

7.1.1.3 Cells voltages during the exposure to 2 ppm of DMS

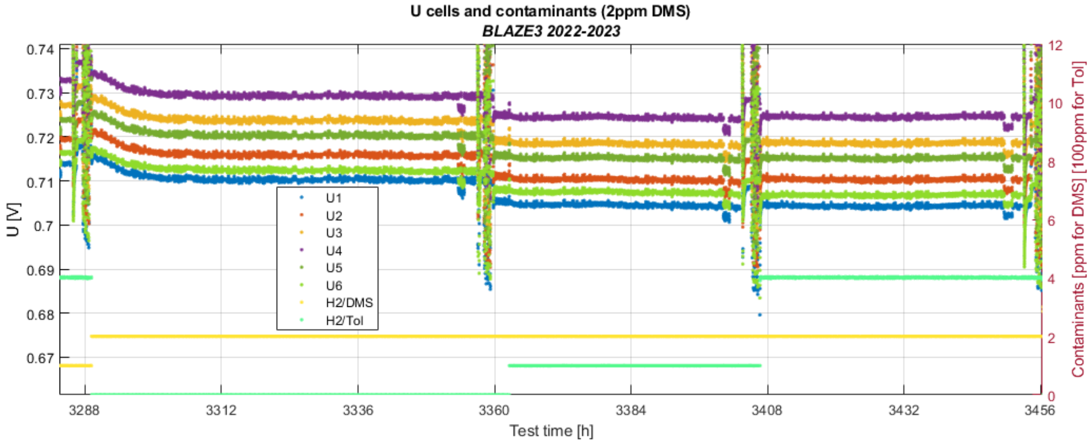

Figure 50: Contamination phase = 2 ppm DMS. Cell potentials on the left axis. DMS and toluene concentration on the right axis (read 100 ppm and 400 ppm for the toluene concentration.)

The current with DMS was 31.7A and corrected at 3360h, when toluene was added, to 32 A.

7.1.1.4 Cells voltages during the exposure to 3 ppm of DMS

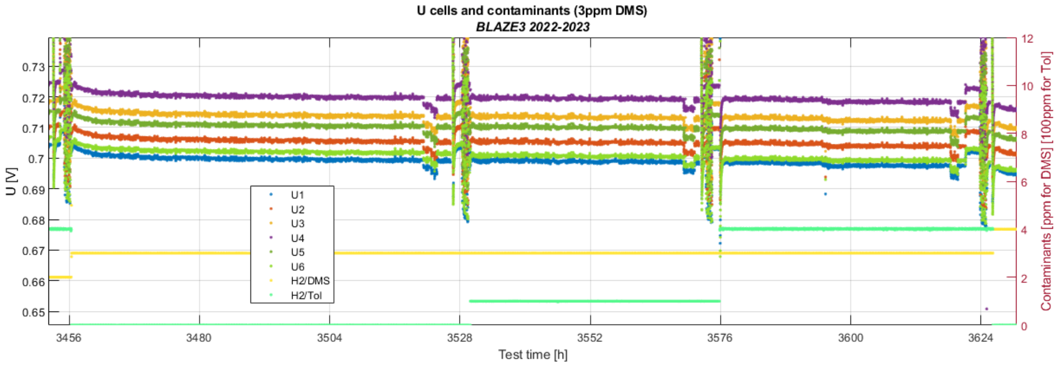

The current set point was held to 32 A throughout the whole phase.

7.1.1.5 Cell voltages during the exposure to 4 ppm of DMS

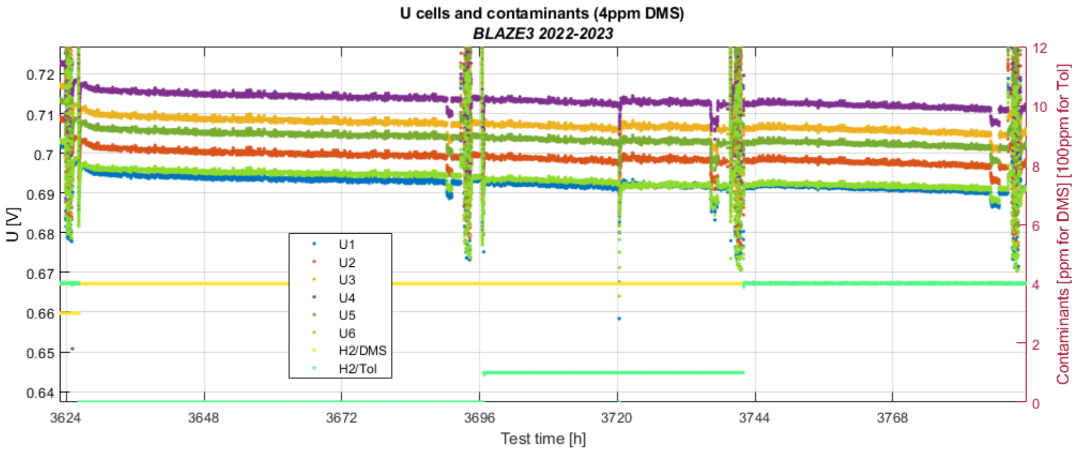

The current set point was held to 32 A throughout the whole phase.

7.1.1.6 H_2S measurement from GC

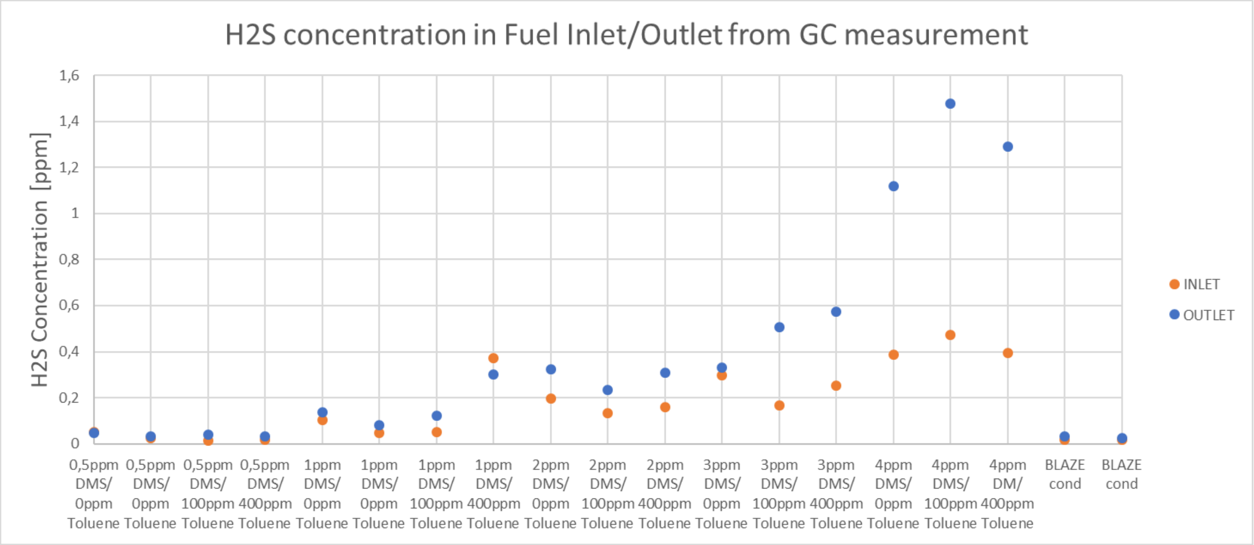

Figure 51: Dry inlet and outlet anode H_2S concentration during the contamination phase. Measurement from the GC.

7.1.1.7 Error comparison on the areas from Bode plot and DRT analysis (peakfit.m)

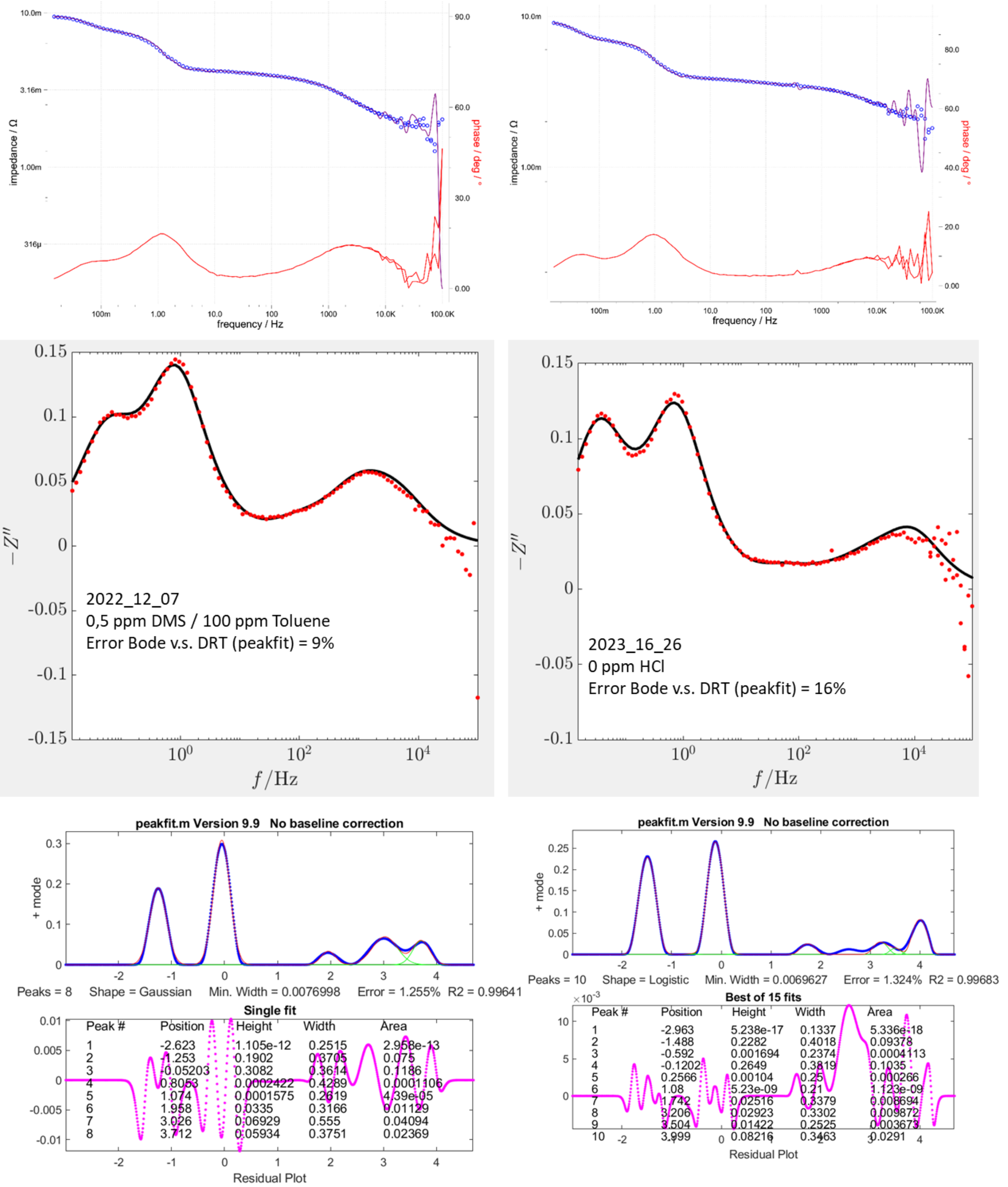

2022_12_07
0,5 ppm DMS / 100 ppm Toluene
Error Bode v.s. DRT (peakfit) = 9%

2023_16_26
0 ppm HCl
Error Bode v.s. DRT (peakfit) = 16%

```
peakfit.m Version 9.9   No baseline correction
Peaks = 8   Shape = Gaussian   Min. Width = 0.0076998   Error = 1.255%  R2 = 0.99641
Single fit
Peak #      Position    Height       Width     Area
1           -2.623      1.105e-12    0.2515    2.958e-13
2           -1.253      0.1902       0.3705    0.075
3           -0.05203    0.3082       0.3614    0.1186
4           0.8053      0.0002422    0.4289    0.0001106
5           1.074       0.0001575    0.2619    4.39e-05
6           1.958       0.0335       0.3166    0.01129
7           3.026       0.06929      0.555     0.04094
8           3.712       0.05934      0.3751    0.02369
```

```
peakfit.m Version 9.9   No baseline correction
Peaks = 10   Shape = Logistic   Min. Width = 0.0069627   Error = 1.324%  R2 = 0.99683
Best of 15 fits
Peak #      Position    Height       Width     Area
1           -2.963      5.238e-17    0.1337    5.336e-18
2           -1.488      0.2282       0.4018    0.09378
3           -0.592      0.001694     0.2374    0.0004113
4           -0.1202     0.2649       0.3819    0.1035
5           0.2566      0.00104      0.25      0.000266
6           1.08        5.23e-09     0.21      1.123e-09
7           1.742       0.02516      0.3379    0.008694
8           3.206       0.02923      0.3302    0.009872
9           3.504       0.01422      0.2525    0.003673
10          3.999       0.08216      0.3463    0.0291
```

Figure 52: Left: 0.5 ppm DMS / 100 ppm toluene at 9% error. Right: 0 ppm HCl at 16% error. Top: Z-HIT test (red = phase, blue = impedance, purple = impedance from Z-HIT), Middle: DRT tool fit (red = raw data, black = fit), Bottom: Peakfit (blue= data from DRT tool, red=fit, green= individual peak fit)